HHS Public Access

Author manuscript

Coord Chem Rev. Author manuscript; available in PMC 2021 May 15.

Published in final edited form as:

Coord Chem Rev. 2020 May 15; 410: . doi:10.1016/j.ccr.2020.213181.

Biomedical Applications of Metal Organic Polygons and Polyhedra (MOPs)

Soumen K. Samanta[a,b], **Lyle Isaacs**[a]

[a]Department of Chemistry and Biochemistry, University of Maryland, College Park, Maryland 20742 United States.

[b]School of Chemistry, University of Bristol, Cantock's Close, United Kingdom, BS8 1TS.

Abstract

Since the discovery and structural characterization of metal organic polygons and polyhedra (**MOPs**), scientists have explored their potential in various applications like catalysis, separation, storage, and sensing. In recent years, scientists have explored the potential of supramolecular **MOPs** in biomedical application. Pioneering works by Ehrlich, Rosenberg, Lippard, Stang and others have demonstrated that **MOPs** have great potential as a novel class of metallo–therapeutics that can deliver cargoes (drugs and dyes) selectively. In this article, we document the progress made over the past two decades on the biomedical applications of **MOPs** and discuss the future prospects of this emerging field.

Keywords

MOPs; Metallotherapeutics; Antitumor Agents; Drug Formulation; Drug Delivery

Introduction

Drug discovery, formulation and delivery are major thrusts in chemistry, medicine and biology.[1, 2] Despite the overwhelming presence of (synthetic) organic small molecule drugs and biopharmaceutical drugs in the market, metal–based drugs and dietary supplements are now becoming more prevalent.[3-5] The reaction and interaction between biomolecular entities and organic molecules are common in biology, as are their interactions with metal ions which are known to intimately control biological functions.[4, 6] Although Nature limited human physiology to few bioavailable metal ions – mostly alkali (Na, K), alkaline earth (Mg, Ca) and first row transition (Fe, Ni, Cu, Mn, Zn, Co) metal ions – many

LIsaacs@umd.edu and samantachem@gmail.com.

CRediT Author Statement

Soumen K. Samanta: Conceptualization, Formal Analysis, Investigation, Roles/writing – original draft, Writing-review/editing.
Lyle Isaacs: Conceptualization, Formal Analysis, Supervision, Investigation, Roles/writing – original draft, Writing-review/editing.

Conflict of Interests

Authors declare that there are no conflict of interests.

biomolecules have the capacity to interact with second and third row transition metal ions and exhibit novel biological responses which are particularly useful to diagnose and treat diseases. One of the first therapeutic metallodrugs was salvarsan, an arsenic–based antimicrobial agent developed by Paul Ehrlich in 1912, as an effective treatment against syphilis.[7] Later in 1965, the serendipitous discovery of the inhibitory ability of *cis*–diammine–dichloroplatinum(II) complex (*cis*-$[Pt(NH_3)_2Cl_2]$) on *E. coli* cell division by Barnett Rosenberg and Loretto VanCamp[8, 9] marked the beginning of the modern era of metallotherapeutics. Subsequently, the *US Food and Drug Administration* approved the use of *cis*–$[Pt(NH_3)_2Cl_2]$ under the brand name *cisplatin to treat testicular cancer. Cisplatin* has spurred the imaginations of numerous scientists to investigate the properties of other metal–coordination and organometallic complexes to as potential therapeutic metallodrugs. The Ptmetal center of *cisplatin* binds covalently to DNA to form *cisplatin*•DNA adducts leading to replication arrest, transcription inhibition, cell-cycle arrest and apoptosis.[10, 11] Two other platinum–based metallodrugs that are approved for cancer treatment are oxaliplatin and carboplatin, while several other platinum–based drugs (e.g. nedaplatin, lobaplatin, heptaplatin and satraplatin) are in clinical trials (Chart 1).[12] Several non–platinum metal–coordination and organometallic complexes also showed great promises as novel metallo–pharmaceuticals and some of them are in clinical trials, currently.[4, 6] Metal complexes featuring Gallium (Ga), Ruthenium (Ru), Rhodium (Rh), Titanium (Ti), Vanadium (V), Tin (Sn), Silver (Ag), Arsenic (As), Antimony (Sb), Bismuth (Bi), Gold (Au), Cobalt (Co), Manganese (Mn), Iron (Fe) complexes have also been studied extensively studied as potential metallopharmaceticals (e.g. anticancer, antiarthritic, antidiabetes, antiviral, antimicrobial and antiparasitics).[4, 5] For example, the arsenic containing drug, melarsoprol is currently used against human African sleeping sickness.[5] The antimony and bismuth containing drugs sodium stibogluconate, melglumine antimoniate, and colloidal bismuth subcitrate (CBS) are used against microbial and parasitic infections (Chart 1).[5] Coordination complexes of gallium and ruthenium have also shown great promise as anticancer agents and several of them (*e.g.* NAMI–A, KP1019 and NP 300) are in clinical trials.[5] Organometallic complexes also showed high antitumor activity, with some arene–ruthenium complexes exhibiting very high anticancer activity.[13] Accordingly, significant effort has been spent to develop new organometallic arene–ruthenium complexes as novel anticancer agents. For example, RM175, [(η^6–biphenyl)(ethylenediamine)ruthenium(II)–chloride][14, 15] and RAPTA-C, [(η^6-para-cymene-(1,3,5-triaza-7-phosphaadamantane)ruthenium(II)-dichloride][16, 17] (Chart 1) exhibited promising anticancer activity in various *in vitro* and *in vivo* experiments. These findings will continuously inspire future research on developing new metallodrugs.

Despite the tremendous efforts during drug development, the real-world applications of many drugs are limited by to poor therapeutic efficacy and dangerous or even fatal side effects.[18] Often, drug molecules are rapidly metabolized or cleared from systemic circulation, which requires frequent administration of drugs.[19, 20] To circumvent such problems scientists have adopted novel strategies to encapsulate drugs within container molecules to protect them from degradation and rapid clearance. The pharmaceutical chemistry community has developed numerous strategies to formulate and deliver drugs.[21] For example, small molecule–based (low molecular weight) delivery systems are known to

prevent degradation and to deliver drugs, thus significantly altering the pharmacokinetic and biodistribution profiles of drugs.[1, 2, 22-24] For example, the β-cyclodextrin derivative *Captisol* (Chart 2) is used to formulate many water insoluble drugs for human administration. Recently Isaacs and coworkers demonstrated that acyclic cucurbit[n]uril–based small molecular containers are promising candidates for formulation and delivery of numerous water insoluble drugs (Chart 2).[23-25] Conversely, large nanoparticle–based systems have been explored extensively and offer many advantages.[20, 26, 27] For example, it is believed that drug delivery systems with diameters ≥ 6 nm avoid rapid kidney clearance which increases blood circulation time.[28, 29] In addition, large nanoparticles benefit from the enhanced permeability and retention (EPR) effect, which results in selective accumulation of nanoparticles in the tumor compartment, thus improving distribution profiles. Numerous nanoparticle–based systems (e.g. polymersomes, dendrimers, inorganic and polymeric nanoparticles, *etc.*) have been reported in the literature for drug formulations and selective drug delivery to tumors.[26, 27, 30, 31] Several nanoparticle formulations (e.g. liposomal, polymeric micellar formulations) of drugs like doxorubicin, paclitaxel, neocarzinostatin have been approved by the US–FDA for clinical use. The liposomal formulation of doxorubicin, which greatly reduces its cardiotoxicity, is approved by the US–FDA as Doxil® (Chart 2) for cancer treatment.[32] Several other nanoparticle formulations of many potent drugs (like cyclodextrin–PEG micelle for camptothecin, lipid nanoparticles for SiRNA) are currently in clinical trials. Liposome nanoparticle formulations of cisplatin (marketed as Lipoplatin) and oxaliplatin (marketed as Lipoxal) which are thought to alleviate the side effects of cisplatin and oxaliplatin, are currently in clinical trials (Chart 2). Advanced drug delivery systems provide a means to fully exploit the potential of platinum and other metal ion–based antitumor agents.[33-35]

Metal–coordination driven self–assembly of metal ions or clusters in combination with multidentate organic ligands has allowed the creation of fascinating families of metal organic materials *e.g.* polygons, discrete polyhedra, coordination polymers and metal organic frameworks (**MOFs**).[36-38] Metal organic polygons and polyhedra (**MOPs**) are discrete macrocycles and cages, respectively. Coordination polymers are 1D, 2D and 3D extended networks of metal ligand assemblies. **MOFs** are crystalline polymeric network of metal ligand assemblies but with potential inner porosity. Over last two decades, a tremendous diversity of metal organic materials have been synthesized and explored for various applications e.g. catalysis, gas storage, separation, sensing, and drug delivery.[39-54] The use of metal organic materials in the field of nanomedicine is beginning to unfold. Self–assembled metal organic materials are composed of a multiplicity of metal–based coordination complexes. Therrein *et al* envisaged that self–assembled **MOPs** – similar to small molecule coordination complexes – might display enhanced anticancer activity.[55] For example, Therrein and coworkers studied the antitumor activity of arene–ruthenium based **MOPs** (**MOP 1**–**9**) and whereas Stang *et al* studied the cytotoxicity of arene–ruthenium and platinum–based **MOPs** (**MOP 10**–**51**).[56] In an interesting example, Tocher *et al* investigated the anticancer activity of the ruthenium–based organometallic complex $Ru(\eta^6\text{-}C_6H_6)(metronidazole)Cl_2$ (metronidazole = 1-hydroxyethyl-2-methyl-5-nitroimidazole) where metronidazole, an antibiotic was used as a ligand coordinated to Ru(II) metal center.[57] Interestingly, the Ru(II) complex exhibited higher potency toward

cancer cells compared to metronidazole alone indicating the enhancement of anticancer activity of metronidazole drug upon inclusion of Ru(II) metal ion. Self–assembled **MOPs** are known to bind a wide range of guest molecules through several non–covalent interactions (like hydrophobic, hydrogen bonding, electrostatic interactions). In his pioneering work, Therrein *et al* showed that arene–ruthenium based **MOP** can be utilized to encapsulate and deliver [M(acac)$_2$] (M = Pd, Pt) complexes to cancer cells.[55] Later, this strategy was adopted by other scientists to deliver theranostic agents to cancer cells, demonstrating the potential of **MOPs** as drug delivery vehicles.[56, 58] Along with **MOPs**, metal organic frameworks (**MOFs**) were also extensively investigated for biomedical applications. In 2006, Ferey *et al* first demonstrated that **MOFs** can be used to formulate and deliver therapeutic drugs.[59, 60] Following his pioneering work, extensive research work has been done on this topic, most notably by Prof. Wenbin Lin.[61-68] In this review, we restrict ourselves to discussion of the use of discrete metal organic polygons and polyhedra (**MOPs**) in biomedical applications.[56, 58, 69] In next two sections, we discuss the use of **MOPs** as theranostic agents and drug delivery vehicles. In this review article, we referred all metal organic structures as **MOPs** for clarity and self-consistency, though they were designated differently like metallacycles, metal-organic cages or metal-organic knots by the authors in the original papers.

MOPs as Theranostic Agents

Therrein *et. al*. first investigated antitumor activity of self–assembled coordination cages incorporating *p*-cymene ruthenium building blocks bridged by 2,5-dioxydo-1,4-benzoquinonato (dobq) spacer.[55] The ruthenium-based **MOP 1** (Figure 1A) was synthesized by reacting 2,4,6-tris(pyridine-4-yl)-1,3,5-triazine with the dichloro salt of **dobq** diruthenium spacer. **MOP 1** was stable in D_2O and its aqueous solution exhibited cytotoxicity (IC_{50} = 23 μM) toward human ovarian cancer cells (A2780). A detailed investigation of the reactivity and stability of **MOP 1** with several biological ligands like amino acids, ascorbic acid and glutathione was performed to determine the origin of cytotoxicity.[70] The results of NMR and ESI established that amino acids like arginine, histidine and lysine caused the degradation of **MOP 1** while methionine had no effect. **MOP 1** catalyzes the oxidation of ascorbic acid to dihydroascorbic acid and glutathione (GSH) to disulfide, which provides a cause of the *in vitro* cytotoxicity of ruthenium–based **MOP 1**.

Different ruthenium and platinum–based **MOPs** were prepared by Therrein, Stang and others who systematically studied their *in vitro* cytotoxicities. For example, Stang and Chi *et. al.* prepared four different types of ruthenium–based self–assembled [3+2] tetragonal prisms (**MOP 2-5**) by separately reacting 1,3,5-tris(pyridine-4-ylethynyl)benzene (**5**) with four different diruthenium organometallic spacers (**1** – **4**, Figure 1A).[71] Cell viability studies were performed against five different cell lines (SK-hep-1 (liver), HeLa (cervix), HCT-15 (colon), A-549 (lung), and MDA-MB-231 (breast). Tetragonal prisms **MOP2** (with **oxalate**-based diruthenium spacer) and **MOP 4** (with **donq**-based diruthenium spacer) are found to be active, whereas **dobq** and **dotq**-based diruthenium containing tetragonal prisms, **MOP 3** and **MOP 5**, respectively, do not show any activity (Table 1). No correlation between the cytotoxicities of **MOPs** and the size of aromatic system of diruthenium spacers

was found. Interestingly, **MOP 4** was as cytotoxic or more cytotoxic than cisplatin toward several cell lines (Table 1).

Although the detailed reasons are not known, it is clear that particular combination of donors and diruthenium spacers is responsible for low IC_{50} value of tetragonal prisms. The most diverse subset of ruthenium–based **MOPs** studied to date is based on a [2+2] self–assembled scaffold. Navarro, Barea and coworkers[72] reported the preparation of [2+2] ruthenium–based polygon (**MOP**) from rigid 4,4'-bipyridine and diruthenium spacer ($[(Cymene)_2Ru_2(CF_3SO_3)_2(Hoxonato)]_2$). This **MOP** binds noncovalently with DNA, inducing significant conformational change in the biomolecule and exhibited antitumor activity (IC_{50} = 4.6 μM) toward human ovarian cancer cell line A2780cisR which showed acquired resistant to cisplatin. Later, Therrein and coworkers[73] prepared several cationic arene-ruthenium based [2+2] **MOPs** from bipyridine (**bpy**) and 1,2-[bis(4-pyridyl)ethylene] (**7**) ligands (Figure 1B). Cytotoxicity studies showed that **MOPs** containing 1,2-[bis(4-pyridyl)ethylene] ligand (IC_{50} = 6 μM for **MOP 7**; IC_{50} = 4 μM for **MOP 9**) are more cytotoxic than **MOPs** containing 4,4′-bipyridine (IC_{50} = 66 μM for **MOP**; IC_{50} = 27 μM **MOP 8**) toward human ovarian cancer cells, A2780. This study demonstrated the correlation between structural properties and observed cytotoxicities of ruthenium–based polygons.

Stang, Chi and coworkers[74] reported several [2+2] metal organic polygons (**MOPs**), prepared from four different type of diruthenium spacers (**oxalato, dobq, donq, dotq**) and four different pyridyl-based donor ligands (Figure 2A). The simplest assemblies are made from 4–pyridyl building blocks, **8**–**11**. The cytotoxicity of polygons **MOP 10**–**20** (Table 1) were measured against several human cancer cell lines (SK-hep-1, HeLa, HCT-15 and AGS). Interestingly, **oxalato** and **dobq**–containing polygons do not show any significant anticancer activity. The larger polygons containing **donq** and **dotq** spacers exhibited higher potency against all cell lines. In particularly, the IC_{50} values for polygons **MOP 19** and **MOP 20** containing Pt-based pyridyl ligand **11** with **donq** and **dotq** spacers are even lower than cisplatin and doxorubicin, (Table 1) which is attributed not to the ruthenium–acceptor but rather to the Pt–containing ligand. Moreover, **oxalato** and **dobq**–containing polygons (**MOP 25** and **MOP 26**) with 3-pyridyl donor-based extended ligand (**13**) have measurable cytotoxicity (Table 1).[75] The rectangle–containing the **dotq**–molecular spacer with extended dipyridyl ligand (**MOP 28**) display higher activity relative to **MOP 24** which contains a shorter dipyridyl ligand. This study suggested that larger–sized assemblies are more active than smaller–sized **MOPs**, though reasons are still unclear and further investigations are needed.

Stang, Chi and coworkers further extended the scope of this work by incorporating additional functional groups in the pyridyl–based ligands like amide groups for H–bonding interactions and azo groups for potential photosensitization (Figure 2A). Several [2+2] polygons (**MOP 29** – **31**) were prepared by reacting **oxalato**– and **donq**–based diruthenium spacer with amide–containing pyridyl ligands (**14** and **15**).[76] Cytotoxicity studies showed that **MOP 31** is highly toxic towards several human cancer cell lines (SK-hep-1, HeLa, HCT-15 and A-549 and MDA-MB-231) than **MOP 29** (Table 1). Similar observations were noticed for azopyridyl–based polygons (**MOP 34**–**49**) prepared from azopyridyl–based

ligands **17**–**20**, with considerably high toxicities found only for **donq**–containing **MOPs** with IC_{50} values ranging from 12 to 37 μM.[77] Another subset of [2+2] **MOPs** were prepared by using asymmetric ligand **16** which results in two isomeric assemblies, namely the head–to–head (HTH) and head–to–tail (HTT) isomers.[78] Reaction of asymmetric ligand **16** with two different diruthenium spacers separately gave **MOP 32** and **MOP 33**, each with a statistical mixtures of both isomers. Once again, large polygon (**MOP 33**) containing **donq**–based diruthenium spacer had the lowest IC_{50} values towards human cancer cell lines (Table 2).

Recently, Stang and Chi developed new diruthenium–based molecular spacer (**21**), prepared from bis–benzimidazole ligand. Reaction of diruthenium spacer, **21** with ditopic (**14**) and ditopic tritopic (**5**) ligands separately gave [2+2] polygon (**MOP 50**) and [3+2] polyhedron (**MOP 51**), respectively, (Figure 2B).[79] Cell viability studies demonstrated that **MOP 51** was more active towards Colo320, H1299 and MCF7 compared to **MOP 50** and cisplatin drug with the exception of A-549 cell in which **MOP 50** was more effective (Table 2). All these studies demonstrated the potential applicability of ruthenium–based **MOPs** for development of new metallo–pharmaceuticals for anticancer treatment. It is noteworthy that arene–ruthenium based **MOPs** exhibit inherent toxicity with IC_{50} values similar with other potent anticancer drugs like cisplatin and doxorubicin.

Very recently, Trabolsi and coworkers demonstrated that interlocked metal organic polyhedra (**MOP 52**) could be novel class of **MOP**–based materials to develop new antitumor agents.[34] The authors synthesized several metal organic trefoil knots featuring Zn(II), Cd(II), Cu(II), Fe(II) and Mn(II) metal ions by self-assembly (Figure 3A). All knots were found to be water soluble and stable under physiological conditions. *In vitro* studies demonstrated that these water soluble metallo-trefoil knots showed high potency against several cancer cell lines (HeLa, A2780, A2780/cis, MDAMB-231, PC3, MCF-7) and for many cases similar to or higher than *cisplatin* (Table 3). Interestingly, these metallo-trefoil knots are less potent toward non cancer cells like HEK 293. Mechanistic studies indicated different mechanistic pathways for the cellular uptake of trefoil knots than *cisplatin*. *Cisplatin* chooses to penetrate cells by a direct diffusion mechanism, which is a less selective uptake mechanism resulting in the high toxicity of *cisplatin* toward normal cells. In contrast, trefoil knots were taken up by a transporter–mediated endocytotsis pathway. The different uptake pathway mechanisms explain the following features – low toxicity of trefoil knots toward HEK293 normal cells due to lower internalization and higher toxicity of these knots toward cisplatin–resistant A2780 cells. All metallo-trefoil knots featured acid–sensitive hydrolyzable imine bonds which hydrolyze at the low pH inside cancer cells to release active metal ions. Mechanistic studies suggest that the reason for cellular toxicity is cell apoptosis. Metallo-trefoil knots elicited higher levels of reactive oxygen species (**ROS**) compared to *cisplatin*, leading to mitochondrial damage–mediated *via* an apoptotic pathway. Consistent with the *in vitro* results, an *in vivo* study on zebrafish embryos showed (Table 3) higher toxicity of metallotrefoil knots (LD_{50} = 4–8 μM) than *cisplatin*, with highest potency of the Cu–based trefoil knot (LD_{50} = 4 μM for **Cu–MOP 52**). This result is also manifested in the mortality rate of zebrafish embryos pre–exposed to metallo-trefoil knots (**MOP 52**). Embroys treated with metal–free trefoil knot survived (Figure 3B) even at 120 hpf (hpf =

hours post fertilization), whereas they were found dead by 48 hpf after pre–exposed to highly potent Cu–based trefoil knot (**Cu–MOP 52**). Intermediate mortality was observed when embroys are pre–exposed to other metallotrefoil knots. This study demonstrated the potential of interlocked metallosupramolecular structures in developing novel antitumor agents.

Similarly, platinum–based self–assembled structures became a logical choice for developing new antitumor agents, due to the high potency of several platinum complexes (*e.g.* cisplatin, oxaliplatin, carboplatin *etc.*) toward various cancer cell lines.[80-82] Fujita and Stang *et. al.* pioneered the preparation of platinum–based polygons and polyhedra using self-assembly.[39] Stang and coworkers first envisaged that platinum–based self–assembled **MOPs** can be used to develop novel antitumor agents. In 2014, they first demonstrated antitumor activities of platinum–based polygons.[83] Reaction of 2,6-bis(pyrid-4-ylethynyl)aniline (**23**) and 2,9-bis[*trans*-$Pt(PEt_3)_2(OTf)$]phenanthrene (**22**) afforded tetranuclear platinum–based rhomboidal polygon, **MOP 53** (Figure 4). **MOP 53** was found to be soluble, stable and highly emissive compared to free ligands **(22** and **23)** in biologically relevant solvent water–DMSO (0.2% vol/vol). The cytotoxicity of platinum–based **MOP 53** was assessed using the standard cell viability assay (3-(4,5-dimethylthiazol-2-yl)-2,5-diphenyltetrazolium bromide, (MTT)) toward HeLa and A549 cells, with free ligand as control. No significant decrease in metabolism was observed suggesting low cytotoxicity of **MOP 53** within the concentration range of 1 nM to 5 μM. Confocal microscopy showed that **MOP 53** remained stable after cellular internalization and did not undergo any photobleaching. Significant tumor volume suppression (64%) was observed from *in vivo* efficacy study (Figure 4) when xenograft tumor–bearing mice of breast cancer MDA–MB–231 were treated with **MOP 53**. This pioneering work demonstrated the promise of platinum–based self–assembled **MOPs** in developing novel antitumor agents.

As previously discussed, EPR effect allows better uptake of large–sized nanoparticles by the tumors. In an interesting example, Stang and coworkers incorporated therapeutic platinum–based **MOP** into polymeric nanoparticles (Figure 4) and studied their uptake behavior both *in vitro* and *in vivo*. Accordingly, rhomboidal platinum–based polygon (**MOP 54**) was synthesized using tetraphenylethene(TPE)–based bispyridyl ligand (**24**).[84] The exohedral amine groups of **MOP 54** were subsequently reacted with N-hydroxysuccinimide–activated carboxylic acid–based cross linker (**25**) to produce polymeric nanoparticles, **NP1** and **NP2** (Figure 4) with diameters of ~ 250 to 310 nm, as characterized by Scanning Electron Microscopy (SEM) and Dynamic Light Scattering (DLS) study. Due to aggregation induced emission of TPE units, the polymeric nanoparticles become highly emissive compared to **MOP 54** or free TPE–based bispyridyl ligand (**24**). Cellular uptake and stability of the **NPs** were investigated by confocal laser scanning microscopy (CLSM). Bright fluorescence was observed in the cytoplasm of the A549R cells after incubation of **NP2** with maximum emission at 521 nm, suggesting the excellent stability of **MOP/NP** in the cellular environment. Fluorescent properties of nanoparticles were further exploited for applications in bioimaging. After *intravenous* injection of **NP2** to MDA-MB-231 tumor–bearing mice, significant accumulation of polymeric nanoparticle **NP2** in the lung was observed from *in*

vivo fluorescence imaging study, demonstrating the applicability of platinum–based self–assembled materials in developing novel theranostic agents.

Later TPE-embedded polygon (**MOP 54**) was further exploited by Stang *et. al.* to prepare novel polymeric nanomaterials to demonstrate codelivery of therapeutic platinum–based drug and potent anticancer drugs like doxorubicin. **MOP 54** was covalently attached (Figure 4) to four amphiphilic copolymers (**26**) through amide bond forming reaction to prepare platinum–based copolymer (**Pt–PBGM–b–POEGM**).[85] **Pt–PBGM–b–POEGM** further self–assembled into highly fluorescent polymeric (**NP3** and **NP4**) and vesicular (**VC**) nanoparticles with diameter of 50 nm and 429 nm, respectively, for **NP3** and **NP4**. The diameter of vesicular nanoparticles was in the range from 0.8–3.0 μM depending on the precise experimental conditions. Importantly, nanoassemblies displayed higher photostability than the conventional fluorophore Lyso Tracker Red. The anticancer activities of **NP3** (IC_{50} = 2.89 μM), **NP4** (IC_{50} = 5.84 μM) and **VC** (IC_{50} = >20 μM) were determined by **MTT** assays. These nanoparticles were able to encapsulate hydrophobic (for **NP3** and **NP4**) or hydrophilic (for **VC**) doxorubicin (DOX). Large–sized nanoparticles were particularly useful due to their selective accumulation inside tumors *via* EPR effect. An *in vivo* efficacy study demonstrated that tumor volume was significantly suppressed (81%), when HeLa tumor–bearing mice were treated with DOX–loaded nanoparticles (DOX@**NP3**) compared to other formulations (cisplatin, DOX, **NP3**). Glutathione (**GSH**)–mediated reduction of azide to amine initiated the cascade elimination reaction which resulted in change in amphiphilicity of copolymer and subsequent disassembly of the nanoparticles allowing codelivery of doxorubicin and platinum–based **MOP** to the tumors leading to better therapeutic efficacy.

Large nanoparticles equipped with targeting ligands benefit from both passive targeting (*via* EPR effect) and active targeting (*via* specific recognition of cellular receptors by targeting ligands), leading to better therapeutic efficacy compared to nanoparticles without targeted ligands.[86] Stang *et al* studied this phenomenon by encapsulating therapeutic platinum–based **MOP** within supramolecular nanoparticles equipped with targeting ligands (Figure 5A).[87] Self-assembly of TPE–based tetrapyridyl ligand (**27**), linear dicarboxylate spacer (**28**) and $Pt(PEt_3)_2(OTf)_2$ afforded tetragonal prism (**MOP 55**). **MOP 55** is highly fluorescent due to the presence of TPE units. **MOP 55** was encapsulated within the hydrophobic core of spherical micelles prepared from a mixture of 1,2-distearoyl-phosphatidylethanolamine/polyethylene glycol conjugates (*m*PEG-DSPE and biotin-PEG-DSPE). **MOP**–loaded nanoparticles (**MNP 1**) with average diameter of 35 nm showed excellent stability in biological environment due to the presence of PEG groups. Biotin moieties attached to the nanoparticles enabled the targeting ability of **MNP 1**. Confocal laser scanning microscopy and flow cytometry studies demonstrated that receptor (biotin)–mediated selective uptake of **MNP 1** by HeLa and HepG2 cells (with overexpressing biotin receptors) compared to normal cells, CHO and HEK-293. **MNP 1** exhibited enhanced cytotoxicity toward HeLa and HepG2 cells. Pharmacokinetic study showed that half-life circulation of **MNP 1** was much higher than cisplatin, oxaliplatin and carboplatin, demonstrating enhanced efficacy of **MOP 55** over conventional platinum-based antitumor agents. Moreover, significant accumulation of **MNP 1** was observed in the tumor compared

to other platinum antitumor agents. Low uptake by the kidney, liver and spleen demonstrated the low cytotoxicity toward these organs. Interestingly, the bright fluorescence of **MNP 1** allowed the authors to use it as an imaging agent. *In vivo* fluorescence imaging study showed higher signal intensity at the tumor compared to other organs, indicating passive targeting *via* EPR effect in operation. Additionally, **MNP 1** significantly suppressed tumor volume compared to conventional platinum antitumor drugs. Both *in vitro* and *in vivo* studies demonstrated that platinum–containing self–assembled **MOP 55** was ideally suited to be included in the list of promising platinum-containing antitumor drugs and thus requires further investigations.

Stang and coworkers further demonstrated the possibility of platinum–based **MOPs** in combination therapy – chemotherapy and photodynamic therapy (PDT).[88] PDT is an effective cancer treatment approach which is minimally invasive in nature and with low side effects. Energy transfer from a light–excited photosensitizer to molecular oxygen ($^3O_2$) produces toxic singlet oxygen ($^1O_2$) which kills cancer cells. Porphyrins are extensively used as photosensitizers. [89-91] Accordingly, porphyrin–based platinum–containing tetragonal prism, **MOP 56** was prepared (Figure 5B) by self–assembly of tetrapyridyl porphyrin (**29**), disodium terephthalate salt (**30**) and therapeutic $(PEt_3)_2Pt(OTf)_2$. The therapeutic efficacy of **MOP 56** was investigated after its encapsulation within hydrophobic core of nanoparticles prepared from mPEG-b-PEBP and RGD-PEG-b-PEBP. The diameter of **MOP**–loaded nanoparticles (**MNP 2**) is 40–80 nm according to dynamic light scattering (DLS). The loading capacity of the formulations was estimated to be 46% (weight:weight). **MNP 2** showed long blood circulation time (2.18 h half-life) and high tumor uptake due to the EPR effect of the large nanoparticles and active targeting ability by virtue of the c–RGD groups. Interestingly, the $^1O_2$ production quantum yield of porphyrin embedded within **MNP 2** could be exploited by the authors for photodynamic therapy (PDT) and near-infrared fluorescence imaging (NIRFI). Confocal laser scanning microscopy (CLSM) and flow cytometry study showed that U87MG cells (overexpressing $\alpha_v\beta_3$ integrin) exhibited uptake of **MNP 2** compared to **MNP** without RGD, indicating receptor–mediated endocytosis for **MNP 2**. Accordingly, **MNP 2** was exploited for dual therapy – chemotherapy and PDT, exhibiting synergistic efficacy both *in vitro* and *in vivo*. Significant tumor suppression was observed after a single–dose injection against U87MG tumor models. Chelation of ^{64}Cu or paramagnetic Mn within the porphyrin macrocycle of **MOP 56** allowed **MNP 2** to be useful for positron emission tomography (PET) and magnetic resonance imaging (MRI) for precise diagnosis of tumor as well as real-time monitoring of bio-distribution and excretion of MNPs. This study provides a platform for the future development of multifunctional theranostics. Taken as a whole, the series of examples discussed above establishes the great promise of supramolecular **MOPs** in developing novel theranostic agents; further development in terms of both new chemical entity preparation and biological (*in vitro* and *in vivo*) studies are ongoing in many labs.[56, 58, 92-94]

MOPs as Delivery Vehicles

MOPs with well–defined cavities are suitable carriers for delivering drug molecules to tumors and a potentially powerful addition to the toolbox of drug delivery systems. This

strategy was first developed by Therrein *et al* in a supramolecular coordination structure to encapsulate and deliver anticancer drugs to cancer cells. For this study, Therrien and coworkers used an arene–ruthenium based trigonal prism, self–assembled from *p*–cymeneruthenium–based metal fragment and pyridyl donors as pioneered by Süss–Fink and coworkers, as the nanocarrier. [55] Self–assembly of two trispyridyl ligands with three diruthenium organometallic complex gave a trigonal prism (**MOP 1**) with a well–defined cavity. Trigonal prism, **MOP 1** was able to encapsulate [(*acac*)$_2$M] (M = Pd, Pt; *acac* = acetylacetonato, Figure 6C) as observed by X–ray crystallography. ^{1}H NMR study showed excellent aqueous stability of **MOP 1** and its host-guest complexes ([(acac)$_2$M]@**MOP 1**). Prolonged aqueous exposure triggered the partial release of guests from the **MOP 1**. [(acac)$_2$Pd] guest is released to a greater extent from **MOP 1** compared to [(acac)$_2$Pd] guest. The free complexes [(acac)$_2$M] (M = Pd, Pt) which are hydrophobic did not exhibit any cytotoxicities toward ovarian cancer cells, A2780. On the other hand, the host–guest complexes (IC_{50} = 12 μM for [(acac)$_2$Pt@**MOP 1**]; 1 μM for [(acac)$_2$Pd@**MOP 1**]) were substantially more cytotoxic than **MOP 1** (IC_{50} = 23 μM). This study demonstrated that water soluble trigonal prism, **MOP 1** has ability to transport water insoluble drugs ([(acac)$_2$M]) to the cancer cells by forming host–guest complexes and to release the drugs after cell internalization to exhibit their toxicity.

Therrien and coworkers further explored the encapsulation properties of the Ru–based cage **MOP 1** toward several fluorescent pyrene derivatives to demonstrate the ability of **MOP** as delivery vehicle and to monitor the uptake and release of anticancer drugs in cellular environment.[95] **MOP 1** was able to encapsulate series of pyrene derivatives (Figure 6A) with diverse functional groups within its cavity, as evidenced by ^{1}H NMR, DOSY NMR and ESI-MS. Antitumor activities of **MOP 1** and its host–guest complexes (pyrenes@**MOP 1**) were studied in human A2780 ovarian cancer cells. The host–guest complexes exhibited lower IC_{50} values compared to the empty cage **MOP 1** (IC_{50} = 23 μM). Two of the pyrene derivatives – sulfonamide containing pyrene (carbonic anhydrase inhibitor, IC_{50} = 2 μM) and ethacrynamide containing pyrene (glutathione transferase inhibitor, IC_{50} = 3 μM), upon forming complexes with **MOP 1** exhibited similar cytotoxicity (Table 4) to *cisplatin* drug (IC_{50} = 1.6 μM). The precise structure of the pyrene derivatives greatly influenced the *in vitro* cytotoxicity of the host–guest system. By attaching appropriate functional groups (e.g. ethacrynamide, sulfonamide, floxuridine) onto pyrene, ruthenium-based highly toxic materials were prepared.

By exploiting this strategy, Therrein and Kim *et. al*. were able to demonstrate the delivery of highly potent anticancer drugs like floxuridine to cancer cells.[96] Accordingly, a prodrug of floxuridine which is a synthetic antitumor nucleoside was derivatized with a pyrene tag. The floxuridine prodrug binds to **MOP 1** by virtue of the pyrene encapsulation ability of the **MOP** to produce floxuridine–prodrug@**MOP 1** (Figure 6A). In contrast to other clinically used floxuridine compounds, floxuridine–prodrug@**MOP 1** is water soluble. The complex is found to be stable in aqueous–biological media and under ESI–MS condition. The antiproliferative activity of **MOP 1** and the host–guest complex (floxuridine-prodrug@**MOP 1**) were tested against human ovarian A2780 and A2780cisR cancer cell lines using the MTT assay. The floxuridine-prodrug@**MOP 1** complex (IC_{50} = 0.3 μM) exhibited higher

toxicity compared to vacant cage **MOP 1** (IC_{50} = 23 μM). This type of host–guest system can be considered as alternative therapeutic of the parent drug floxuridine which suffers poor cellular uptake and bioavailability due to poor water solubility.

After successfully demonstrating the ability of ruthenium–based **MOP 1** to deliver anticancer drugs to the cancer cells, Dyson and Therrein *et al* studied the mechanism of drug release from **MOPs** after cellular internalization.[97] It was observed that encapsulation of the intrinsically fluorescent pyrenyl compound, 1-(4,6-dichloro-1,3,5-triazin-2-yl)pyrene inside **MOP1** led to the fluorescence quenching of the pyrenyl derivatives. This property was exploited to study the intracellular drug release mechanism by using fluorescence microscopy (Figure 6B). Cell viability study on human ovarian A2780 cancer cells showed significantly lower cytotoxicity for the host–guest complex (IC_{50} = 6 μM) compared to both free **MOP 1** (IC_{50} =16 μM) and free pyrenyl derivative (IC_{50} = >20 μM), further demonstrating the cage mediated cellular uptake of the poorly water soluble pyrenyl derivative. At pH 2 or pH 7, no guest release was observed by fluorescence microscopy, whereas at pH 12 the pyrenyl derivative was released from the cage due to the destruction of **MOP 1**. Fluorescence microscopy images showed enhanced fluorescence intensity inside the cells following the treatment with host–guest complex (Figure 6B). Moreover, mechanistic investigations showed that the uptake of the host–guest complex does not correlate linearly with the incubation time or the concentration of the complex, indicating the cellular uptake via an assisted diffusion pathway. Cisplatin displays similar uptake pathways, in which cellular machineries like transporters or receptors are partly involved.

Pioneering works by Therrein and coworkers demonstrated that ruthenium–based **MOPs** can function as antitumor agent alone and also as nanocarriers to deliver other antitumor drugs to the cancer cells, thus improving the therapeutic efficacy of the drugs. Interestingly, the synergistic effect of drugs and **MOPs** may find applications in future in combination therapy.

Later, Crowley and coworkers showed that other palladium–based **MOPs** can also be utilized to deliver therapeutic drugs.[98] Self–assembly of 2,6-bis(pyridine-3-ylethynyl)pyridine ligand with $[Pd(CH_3CN)_4](BF_4)_2$ in acetonitrile afforded quadruply–stranded dipalladium(II) cage (Pd_2L_4–type) **MOP 57** as evidenced by ^{1}H NMR, HR-ESMS and XRD. **MOP 57** was able to encapsulate two molecules of *cisplatin* drugs within its cavity as demonstrated by ^{1}H NMR, ESI-MS and X-ray crystallography (Figure 7A). The encapsulation complex is stabilized by H–bonding interactions (N–H⋯N and C–H⋯Cl) between host and guest and by metal–metal (Pt.⋯Pt) interactions between the two *cisplatin* molecules. Later, Kuhn, Casini and coworkers[99]studied the anticancer activity of *cisplatin*–loaded **MOP** (another variant of **MOP 57)** toward several human cancer cell lines (A549, SKOV-3 and HepG2). The (*cisplatin*)$_2$@**MOP** complex exhibited higher cytotoxicity (IC_{50} = 1.9 ± 0.5 μM) compared to free *cisplatin* (IC_{50} = 15.4 ± 2.2 μM) and free cage **MOP** (IC_{50} = 11.6 ± 1.7 μM). Additionally, an *ex vivo* study demonstrated that **MOP** alone displays very limited toxicity toward healthy liver tissues according to precision-cut liver slices (PCLS) assay. Overall the encapsulation and biological study demonstrated that palladium–based **MOPs** are very attractive candidates for developing novel drug–delivery systems.

Susceptablity toward degradation and poor water solubility often limit the biological application of **MOPs**, whereas extremely low quantum yield prevented a study of their cellular uptake by fluorescence microscopy. Water solubility was improved by attaching glucose molecules to the Pd_2L_4–type **MOP** and stability was significantly enhanced by PEGylation.[100] Kühn and Casini *et al* made highly fluorescent Pd_2L_4–type **MOPs** by attaching fluorophores like naphthalene, anthracene and ruthenium–pyridine complexes to the *exo*–position of the ligands (L),[101, 102] which will enable studies of their cellular uptake in cancer cells by fluorescence microscopy.

The high kinetic inertness of the Pt–N bond makes platinum–based **MOPs** more stable against degradation compared to Pd–based **MOPs** thus improving their prospects as nanocarriers. Lippard *et al*. demonstrated that Pt_6L_4–type cationic **MOP 58** can be utilized to transport anticancer drugs to cancer cells.[103] Platinum cage **MOP 58** is known to bind four adamantane molecules in its hydrophobic pocket in water. [104] Four molecules of newly synthesized adamantylplatinum(IV) prodrug (**31**) bind to **MOP 58** in D_2O (Figure 7B) as confirmed by ^1H NMR and DOSY NMR. This host–guest complex, (**31**)$_4$@**MOP 58** exhibited micromolar potency (Figure 7C) against human cancer cell lines (A549, A2780, and A2780CP70) and showed higher cytotoxicity (IC_{50} =14.7± 2.8 μM) compared to the free prodrug **31** (IC_{50} = 22.3±1.8 μM) and free cage **MOP 58** (IC_{50} = 57.7±9.2μM). The higher cytotoxicity (Table 5) of the host–guest complex is attributed to the higher cellular uptake of the prodrug as the (**31**)$_4$@**MOP 58** complex compared to free prodrug **31** alone. Interestingly, intracellular reduction of platinum (IV) drugs by ascorbic acid followed by release of active drug *cisplatin* demonstrated the utility of this approach in reducing the fatal side effects of active drugs and improving therapeutic efficacy *in vivo*.

The selective transport of therapeutics to the tumor is one of the major challenges in nanomedicine. Targeting nanocarriers selectively to the tumors depends on many factors, but the size of the nanocarrier is an important one. As previously discussed, large–sized nanocarriers (> 6–100 nm)[28, 29] often benefit from EPR effect which lead to the selective accumulation of the cargo–loaded nanocarriers in the tumors. The **MOP**–based nanocarriers described above are rather small with diameters ≤ 2 nm. Despite their abilities to transport anticancer drugs to cancer cells *in vitro*, their utility in *in vivo* applications have not been established. Large–sized **MOP**–based nanocarriers will be useful for demonstrating the passive targeting (*via* EPR effect) effect *in vivo*. The groups of Fujita and Yaghi developed elegant strategies to prepare large–sized MOPs (diameter ≈ 3-10 nm) using self–assembly. [37, 105, 106] These **MOPs** are ideally suitable for developing novel drug delivery systems.

Yaghi *et al* demonstrated the preparation of copper(II)–based porous cuboctahedron cage by reacting with 1,3-dibenzenedicarboxylic acid with $Cu(NO_3)_2$ in mixture of DMF and ethanol.[106] This porous cage is composed of 12 dicopper paddlewheel clusters and 24 isophthalate moieties. The relatively large size of such porous cages (diameter ~ 3–4 nm) makes them potentially a good scaffold for developing novel drug delivery vehicles. Zhao *et al* developed a novel drug delivery system based on a copper(II)–containing cuboctahedral cage and was successful in demonstrating the delivery of anticancer drug, 5-fluorouracil (5-FU).[107] A water soluble version of the copper(II)–containing cubooctahedral cage (**MOP 60**) was prepared *via* surface functionalization of 5-(prop-2-ynyloxy)isophthalic acid (**32**)

which delivered cuboctahedral cage (**MOP 59**) with azide–containing PEG5K polymeric material through click chemistry (Figure 7C). Dark field TEM images showed nanoparticles with diameter of ~20 nm, which is much larger than the expected single **MOP 60** molecule, suggesting intermolecular aggregation. The 5–FU drug loading capacity of **MOP 60** was determined to be 4.38% (weight:weight). The 5–FU–loaded **MOP 60** was dialyzed against PBS buffer solution at pH 7.4 at room temperature to study drug release from **MOP 60**. Approximately 20% drug was released over a period of first 2 h followed by an almost flat release curve for next 24 h (Figure 7C) suggesting very slow/no release of drugs. The observed slow release rate may arise due to the strong interaction between the basic site of 5–FU and Lewis acid sites in **MOP 60**. This study demonstrates the ability of **MOP**–based systems to formulate water insoluble drugs which may find *in vivo* applications in the future.

Fujita *et al* demonstrated that self–assembly of bent–shaped bispyridyl ligands with $Pd(NO_3)_2/Pt(NO_3)_2$ afforded large–sized **MOPs** (diameter ~ 3–8 nm).[108] Facile functionalization at the exo/endohedral position of Fujita–type **MOP** make them highly attractive for various applications.[105] Isaacs and coworkers envisaged that Fujita–type $Pd_{12}L_{24}$ large cuboctahedron **MOP** can be exploited for drug delivery applications.[109] Methyl viologen (MV)–studded $Pd_{12}L_{24}$ **MOP 61** was prepared (Figure 8A) by self-assembly of MV–functionalized bispyridyl ligand (**33**) and $Pd(NO_3)_2$ as characterized by ^1H NMR and ESI-MS. The presence of 24 MV groups on the surface made **MOP 61** highly water soluble. Strong binding affinity of cucurbit[n]uril (CB[7] and CB[8]) toward the MVs on the surface of **MOP 61** was exploited to prepare CB[7]– and CB[8]–capped **MOP** as characterized by ^1H, DOSY NMR, and TEM. The TEM images showed that the diameter of CB[n]–capped **MOP** was 5.5 nm. The CB[8]–capped polyhedron (**MOP 62**) was further able to form the heteroternary complex with 2–hydroxy naphthalene derivative. This property was exploited to load **MOP 62** with naphthol derivatized doxorubicin prodrug (**ProDox**) to give **MOP 63**. The hydrazone linkage of ProDox is acid sensitive and was expected to deliver doxorubicin in pH–responsive manner at the slightly acidic pH of tumors. Cell viability assays showed that drug–loaded **MOP 63** was 10–fold more cytotoxic toward HeLa cells (Figure 8C) compared to an equimolar amount of ProDox. Flow cytometry (Figure 8B) and confocal fluorescence microscopy (Figure 8D) showed that enhanced cytotoxicity originates from the combined effect of enhanced cellular uptake of the drug–loaded **MOP 63** and enhanced release of doxorubicin from ProDox. This study demonstrates that larger **MOPs** have the ability to load drugs and deliver to the cancer cells. Such large–sized **MOPs** in drug delivery may benefit from EPR effect for targeting nanoparticles *in vivo*.

Stang and coworkers showed that methyl viologen–functionalized platinum–based metal organic polygon can be synthesized by self–assembly of MV–functionalized dipyridyl donor and tetraethylene glycol–functionalized organoplatinum acceptor.[110] CB[8]–functionalized platinum–based **MOP** was synthesized by capping MV with CB8. Exploiting the heteroternary complexation property of CB[8], curcumin–mediated polymerization of CB[8]–capped **MOP** afforded micrometer–sized honeycomb like network which was subsequently transformed to tapes of diameter 40–80 nm and then to vesicles with an average diameter of 75 nm. UV/Vis measurements showed higher drug release at lower pH

values which suggests the use of platinum–based **MOPs** in drug delivery to cancer cells. Cell viability studies showed that curcumin–loaded vesicles exhibited 100–fold improved cytotoxicity compared to free curcumin toward several cancer cell lines including human melanoma (C32), melanoma of rodents (B16F10), hormone responsive (MCF-7) and triple-negative (MDA-MB231) breast cancer cells.

Despite major progress in nanoparticle–based drug delivery systems, selective delivery of drugs to tumors in a spatio–temporal manner without affecting healthy tissues is still a major challenge. Although the blockbuster drug Doxil® significantly reduced the cardiotoxicity of Dox by encapsulation within liposomal nanoparticles,[32] it suffers from the slow release of doxorubicin (<5% in 24 h)[111] from the liposomes even after accumulation within the tumor, which hampers its efficacy and requires frequent drug administration. Therefore, the development of new drug delivery systems capable of targeted delivery and stimuli–responsive release is highly sought. Isaacs and coworkers have developed a stimuli–responsive **MOP**–based nanocarrier that releases drug (doxorubicin) or dye (nile red) in response to chemical or pH–chemical stimuli.[112] The $Pd1_{12}L_{24}$–type **MOP 64** was prepared by co-assembly of cucurbit[7]uril–modified bispyridyl ligand (**34**), unmodified bispyridyl ligand (**35**), $Pd(NO_3)_2$ and hexanediammonium (**HDA**) guest (Figure 9A). On the outer surface, **MOP 64** is covalently attached to 18 CB[7] units where the CB[7] cavity is occupied by **HDA** guest. The guest recognition property of CB[7] was exploited to generate a hydrophobic environment within the $Pd_{12}L_{24}$ framework of **MOP 64**. When an amphiphilic guest like $C_{18}H_{37}$–**HDA** was used during co–assembly instead of **HDA**, the long alkyl chains non–covalently attached to the CB[7] units sequester themselves within the cavity of **MOP 66** to create a hydrophobic nanoenvironment. Interestingly, stronger binding guests like adamantane ammonium (**ADA**) are able to destroy the hydrophobic environment by displacing the weaker binding hexane diammonium (**HDA**) guest from the CB[7] cavity. This property was utilized to load and trigger the release of encapsulated guests in stimuli–responsive fashion. Hydrophobic guests like nile red (NR) and doxorubicin (DOX) were found to be encapsulated within the hydrophobic environment of **MOP 65** and guest release was triggered by chemical stimuli like **ADA** (Figure 9B). By changing amphiphilic guest to $C_{18}H_{37}$–**BDA** during co–assembly ($C_{18}H_{37}$–**BDA**) afforded **MOP 66**. Adamantane carboxylic acid guest (**ADAc**) is able to displace butane diammonium (**BDA**) from CB[7] at pH 5.8, but not at pH 7.4, making **MOP 66** responsive toward pH–chemical stimulus as well. Fluorescence spectroscopy study showed that ~75% of nile red was released at pH 5.8 when **MOP 66** is probed with **ADAc**. However, only 10% of nile red was released from **MOP 66** at pH 7.4 upon addition of **ADAc**. Similar observation was noticed for guest doxorubicin as well. Considering that the tumor environment is slightly acidic, the pH–responsive behavior of **MOP 66** may make them useful for drug delivery purposes in stimuli–responsive manner. An effort to study stimuli–responsive guest release from **MOP** inside cancer cells was unsuccessful. After the cellular uptake of **NR@MOP 65** (Figure 9C), nile red is released passively without any external additive like **ADA** as observed by fluorescence microscopy (Figure 9D). This study demonstrated that **MOP**–based system is capable of delivering guest in stimuli–responsive fashion, but more robust delivery systems that only actively release drugs are still needed.

While larger–sized drug delivery systems have major advantages over smaller–sized delivery vehicles due to the EPR effect, small–sized delivery vehicles with 2–3 KDa can have similar advantages when they are attached to cell targeting ligands. Active cell targeting can be achieved for such small molecular weight **MOPs** by successfully conjugating cell–specific ligands, including tumor–targeting peptides that recognize tumor–related surface markers such as membrane receptors. Fujita *et al* first demonstrated the preparation of peptide coated **MOP**.[113] Hexapeptide aptamer–modified ligand was reacted with $Pd(NO_3)_2$ to afford 24 hexapeptide aptamers coated self-assembled $Pd_{12}L_{24}$–type **MOP**. Evidence of multiple aptamers on the surface of $Pd_{12}L_{24}$–type **MOP** is further demonstrated by the irreversible immobilization of the nanocage on a Ti surface, which stands in contrast to weak and reversible binding for a single aptamer ligand. Casini *et al* later demonstrated that relatively smaller cages like $Pd_2\mathbf{L}_4$-type **MOP 57** (**L** = 2,6–bis(pyridin–3–ylethynyl)pyridine) can be *exo*-functionalized with peptides.[114] Bioconjugation of the ligand (**L**) with peptides followed by the formation of supramolecular **MOP** afforded peptide functionalized **MOPs** as evidenced by high resolution mass-spectroscopy.

While attaching cell targeting ligands to small cages is beneficial, it will be extremely useful when they are attached to very large cages as they will benefit from both active and passive targeting. Isaacs and coworkers demonstrated that cucurbit[7]uril–functionalized $Pd_{12}L_{24}$–type **MOP** can be successfully post–functionalized with cell targeting small molecules like biotin and peptides like *c*-RGD. [92] Co–assembly of CB[7]–modified bispyridyl ligand (**34**) and cyclooctyne–modified bispyridyl ligand (**36**) with $Pd(NO_3)_2$ and *p*-xylene diammonium (**PXDA**) guest afforded $Pd_{12}L_{24}$–type **MOP 67** (diameter = 6.5–7.0 nm). **MOP 67** is attached to 18 units of cyclooctyne and 6 units of CB[7] whose cavity is occupied by **PXDA** guests (Figure 10A). Post–modification of **MOP 67** with biotin–azide or RGD–azide *via* click chemistry afforded cell targeting ligands–modified $Pd_{12}\mathbf{L}_{24}$–type **MOP 68**. The higher binding affinity of adamantane ammonium toward CB[7] compared to **PXDA** was exploited to functionalize the cage with a fluorescent dye (FITC) by performing guest exchange of **MOP 68** with **Ad–FITC** to afford **MOP 69**. Covalent and non–covalent modifications afforded **MOP 69** which is equipped with both targeting ligands and fluorescent dye molecules on its surface to investigate active targeted delivery to the cancer cells by fluorescence microscopy. U87 glioblastoma cells which express c–RGD binding integrin receptors ($\alpha_v\beta_3$) on cell surfaces, are incubated with c–RGD and FITC–labelled **MOP 69** for 30 mins at −4 °C. Flow cytometry (Figure 10B) study showed that **MOP 69** equipped with c-RGD targeting ligands are better taken up by cells compared to control **MOP** which lacks c–RGD targeting peptide. This example demonstrated the ability of targeting ligands to selectively deliver **MOPs** to cancer cells. Larger **MOPs** equipped with cell targeting ligands will benefit from both passive targeting (EPR effect) and active targeting (receptor–mediated uptake), which will enhance the therapeutic efficacy of the **MOP**–based drug delivery systems *in vivo*.

Conclusion and Outlook

Self–assembled metal organic materials have emerged as novel supramolecular materials for a variety of applications. The use of **MOPs** in biomedical applications is an emerging and

rapidly expanding field of research. Metal organic polygons and polyhedra (**MOPs**) were found to be excellent candidates for developing new antitumor agents. Pioneering works by Stang, Therrein and others demonstrated that both Ru– and Pt–based **MOPs** exhibited cytotoxicities toward various cancer cell lines similar with other potent drugs like cisplatin or doxorubicin. These studies demonstrated that future research work on **MOPs** needs to be done to explore the full potential of **MOPs** as novel antitumor agents. The encapsulation of unmodified drugs and prodrugs within metal organic cages was cleverly exploited to protect and deliver cargoes to cancer cells. The targeted delivery of dyes to cancer cells using **MOPs** demonstrated by Isaacs and coworkers suggested potential applicability of metal organic cages in targeted drug delivery applications. These initial successes suggest that **MOP**–based systems should be more thoroughly investigated for biomedical applications. One challenge of current **MOP**–based drug delivery systems is their modest stability and tendency to fall apart within biologically relevant media. Often integration of **MOPs** with diverse class of chemicals are compulsory for selective delivery of drugs or dye to the desired location. So, the prospect of this field is not only relying on mere exploration of several **MOP**–based systems toward biomedical applications but also their ability to withstand in biological media and other chemical modifications. One future aim of this emerging field of research will be to look for more stable and robust **MOPs**.

Acknowledgements:

Lyle Isaacs thanks the National Institute of Health (CA226830) for financial support.

References

[1]. Mitragotri S, Burke PA, Langer R, Nat. Rev. Drug Discovery 13 (2014) 655–675. [PubMed: 25103255]

[2]. Srinivasarao M, Galliford CV, Low PS, Nat. Rev. Drug Discovery 14 (2015) 203–219. [PubMed: 25698644]

[3]. Hambley TW, Science 318 (2007) 1392–1393. [PubMed: 18048674]

[4]. Clarke MJ, Zhu F, Frasca DR, Chem. Rev 99 (1999) 2511–2534 [PubMed: 11749489]

[5]. Mjos KD, Orvig C, Chem. Rev 114 (2014) 4540–4563. [PubMed: 24456146]

[6]. Jaouen G, John Wiley & Sons: Weinheim, Germany, (2006).

[7]. Ehrlich P, Bertheim A, Ber. Dtsch. Chem. Ges 45 (1912) 756–766.

[8]. Rosenberg B, Van Camp L, Krigas T, Nature 205 (1965) 698–699 [PubMed: 14287410]

[9]. Rosenberg B, Vancamp L, Trosko JE, Mansour VH, Nature 222 (1969) 385–386. [PubMed: 5782119]

[10]. Sherman SE, Lippard SJ, Chem. Rev 87 (1987) 1153–1181.

[11]. Jung Y, Lippard SJ, Chem. Rev 107 (2007) 1387–1407 [PubMed: 17455916]

[12]. Kelland L, Nat. Rev. Cancer 7 (2007) 573–584. [PubMed: 17625587]

[13]. Chatterjee S, Kundu S, Bhattacharyya A, Hartinger CG, Dyson PJ, J. Biol. Inorg. Chem 13 (2008) 1149–1155. [PubMed: 18597125]

[14]. Aird RE, Cummings J, Ritchie AA, Muir M, Morris RE, Chen H, Sadler PJ, Jodrell DI, Br. J. Cancer 86 (2002) 1652–1657. [PubMed: 12085218]

[15]. Bergamo A, Masi A, Peacock AFA, Habtemariam A, Sadler PJ, Sava G, J. Inorg. Biochem 104 (2010) 79–86. [PubMed: 19906432]

[16]. Scolaro C, Bergamo A, Brescacin L, Delfino R, Cocchietto M, Laurenczy G, Geldbach TJ, Sava G, Dyson PJ, J. Med. Chem 48 (2005) 4161–4171. [PubMed: 15943488]

[17]. Ratanaphan A, Temboot P, Dyson PJ, Chemistry & Biodiversity 7 (2010) 1290–1302. [PubMed: 20491084]

[18]. Williams HD, Trevaskis NL, Charman SA, Shanker RM, Charman WN, Pouton CW, Porter CJH, Pharmacol. Rev 65 (2013) 315–499. [PubMed: 23383426]

[19]. Minotti G, Menna P, Salvatorelli E, Cairo G, Gianni L, Pharmacol. Rev 56 (2004) 185–229. [PubMed: 15169927]

[20]. Sun T, Zhang YS, Pang B, Hyun DC, Yang M, Xia Y, Angew. Chem. Int. Ed 53 (2014) 12320–12364.

[21]. Savjani KT, Gajjar AK, Savjani JK, ISRN Pharm. (2012) 195727. [PubMed: 22830056]

[22]. Macartney DH, Isr. J. Chem 51 (2011) 600–615.

[23]. Ma D, Hettiarachchi G, Nguyen D, Zhang B, Wittenberg JB, Zavalij PY, Briken V, Isaacs L, Nat. Chem 4 (2012) 503–510. [PubMed: 22614387]

[24]. Hettiarachchi G, Samanta SK, Falcinelli S, Zhang B, Moncelet D, Isaacs L, Briken V, Mol. Pharmaceutics 13 (2016) 809–818

[25]. Zhang B, Isaacs L, J. Med. Chem 57 (2014) 9554–9563. [PubMed: 25369565]

[26]. Wolinsky JB, Grinstaff MW, Adv. Drug Delivery Rev 60 (2008) 1037–1055.

[27]. Elsabahy M, Heo GS, Lim S-M, Sun G, Wooley KL, Chem. Rev 115 (2015) 10967–11011 [PubMed: 26463640]

[28]. Fang J, Nakamura H, Maeda H, Adv. Drug Delivery Rev 63 (2011) 136–151.

[29]. Longmire M, Choyke PL, Kobayashi H, Nanomedicine 3 (2008) 703–717. [PubMed: 18817471]

[30]. Sengupta S, Eavarone D, Capila I, Zhao G, Watson N, Kiziltepe T, Sasisekharan R, Nature 436 (2005) 568–572 [PubMed: 16049491]

[31]. Kierstead PH, Okochi H, Venditto VJ, Chuong TC, Kivimae S, Fréchet JMJ, Szoka FC, J. Control. Release 213 (2015) 1–9. [PubMed: 26093095]

[32]. Barenholz Y, J. Control. Release 160 (2012) 117–134. [PubMed: 22484195]

[33]. Boulikas T, Expert Opin. Invest. Drugs 18 (2009) 1197–1218.

[34]. Benyettou F, Prakasam T, Ramdas Nair A, Witzel I-I, Alhashimi M, Skorjanc T, Olsen J-C, Sadler KC, Trabolsi A, Chem. Sci 10 (2019) 5884–5892. [PubMed: 31360392]

[35]. Liu D, He C, Wang AZ, Lin W, Int. J. Nanomed 8 (2013) 3309–3319.

[36]. Perry Iv JJ, Perman JA, Zaworotko MJ, Chem. Soc. Rev 38 (2009) 1400–1417. [PubMed: 19384444]

[37]. Tranchemontagne DJ, Mendoza-Cortés JL, O'Keeffe M, Yaghi OM, Chem. Soc. Rev 38 (2009) 1257–1283. [PubMed: 19384437]

[38]. Chakrabarty R, Mukherjee PS, Stang PJ, Chem. Rev 111 (2011) 6810–6918. [PubMed: 21863792]

[39]. Cook TR, Zheng Y-R, Stang PJ, Chem. Rev 113 (2013) 734–777. [PubMed: 23121121]

[40]. De S, Mahata K, Schmittel M, Chem. Soc. Rev 39 (2010) 1555–1575. [PubMed: 20419210]

[41]. Biswas PK, Saha S, Paululat T, Schmittel M, J. Am. Chem. Soc 140 (2018) 9038–9041. [PubMed: 29932653]

[42]. Schmittel M, Chem. Commun 51 (2015) 14956–14968.

[43]. Clever GH, Tashiro S, Shionoya M, J. Am. Chem. Soc 132 (2010) 9973–9975. [PubMed: 20604553]

[44]. Kumari H, Deakyne CA, Atwood JL, Acc. Chem. Res 47 (2014) 3080–3088. [PubMed: 25198830]

[45]. Brown CJ, Toste FD, Bergman RG, Raymond KN, Chem. Rev 115 (2015) 3012–3035. [PubMed: 25898212]

[46]. Wang W, Chen L-J, Wang X-Q, Sun B, Li X, Zhang Y, Shi J, Yu Y, Zhang L, Liu M, Yang H-B, Proc. Natl Acad. Sci. USA 112 (2015) 5597–5601. [PubMed: 25902491]

[47]. Cullen W, Misuraca MC, Hunter CA, Williams NH, Ward MD, Nat. Chem 8 (2016) 231–236. [PubMed: 26892554]

[48]. Wang Q-Q, Gonell S, Leenders SHAM, Dürr M, Ivanović-Burmazović I, Reek JNH, Nat. Chem 8 (2016) 225–230. [PubMed: 26892553]

[49]. Li Z-Y, Zhang Y, Zhang C-W, Chen L-J, Wang C, Tan H, Yu Y, Li X, Yang H-B, J. Am. Chem. Soc 136 (2014) 8577–8589. [PubMed: 24571308]

[50]. Johnson AM, Wiley CA, Young MC, Zhang X, Lyon Y, Julian RR, Hooley RJ, Angew. Chem. Int. Ed 54 (2015) 5641–5645

[51]. Xu L, Wang Y-X, Chen L-J, Yang H-B, Chem. Soc. Rev 44 (2015) 2148–2167 [PubMed: 25723131]

[52]. McConnell AJ, Wood CS, Neelakandan PP, Nitschke JR, Chem. Rev 115 (2015) 7729–7793. [PubMed: 25880789]

[53]. Wang H, Li Y, Yu H, Song B, Lu S, Hao X-Q, Zhang Y, Wang M, Hla S-W, Li X, J. Am. Chem. Soc 141 (2019) 13187–13195. [PubMed: 31345024]

[54]. Song B, Kandapal S, Gu J, Zhang K, Reese A, Ying Y, Wang L, Wang H, Li Y, Wang M, Lu S, Hao X-Q, Li X, Xu B, Li X, Nat. Commun 9 (2018) 4575. [PubMed: 30385754]

[55]. Therrien B, Süss-Fink G, Govindaswamy P, Renfrew AK, Dyson PJ, Angew. Chem. Int. Ed 47 (2008) 3773–3776.

[56]. Cook TR, Vajpayee V, Lee MH, Stang PJ, Chi K-W, Acc. Chem. Res 46 (2013) 2464–2474. [PubMed: 23786636]

[57]. Dale LD, Tocher JH, Dyson TM, Edwards DI, Tocher DA, Anti-Cancer Drug Des. 7 (1992) 3–14.

[58]. Casini A, Woods B, Wenzel M, Inorg. Chem 56 (2017) 14715–14729. [PubMed: 29172467]

[59]. Horcajada P, Serre C, Maurin G, Ramsahye NA, Balas F, Vallet-Regí M, Sebban M, Taulelle F, Férey G, J. Am. Chem. Soc 130 (2008) 6774–6780. [PubMed: 18454528]

[60]. Horcajada P, Serre C, Vallet-Regí M, Sebban M, Taulelle F, Férey G, Angew. Chem. Int. Ed 45 (2006) 5974–5978.

[61]. Della Rocca J, Liu D, Lin W, Acc. Chem. Res 44 (2011) 957–968. [PubMed: 21648429]

[62]. Zhang Y, Yang L, Yan L, Wang G, Liu A, Coord. Chem. Rev 391 (2019) 69–89.

[63]. Cai W, Wang J, Chu C, Chen W, Wu C, Liu G, Adv. Sci 6 (2019) 1801526.

[64]. Chedid G, Yassin A, Nanomaterials 8 (2018) 916.

[65]. Simon-Yarza T, Mielcarek A, Couvreur P, Serre C, Adv. Mater 30 (2018) 1707365.

[66]. Giménez-Marqués M, Hidalgo T, Serre C, Horcajada P, Coord. Chem. Rev 307 (2016) 342–360.

[67]. Lu K, Aung T, Guo N, Weichselbaum R, Lin W, Adv. Mater 30 (2018) 1707634.

[68]. He C, Liu D, Lin W, Chem. Rev 115 (2015) 11079–11108. [PubMed: 26312730]

[69]. Ahmad N, Younus HA, Chughtai AH, Verpoort F, Chem. Soc. Rev 44 (2015) 9–25. [PubMed: 25319756]

[70]. Paul LEH, Therrien B, Furrer J, Inorg. Chem 51 (2012) 1057–1067. [PubMed: 22221272]

[71]. Vajpayee V, Yang YJ, Kang SC, Kim H, Kim IS, Wang M, Stang PJ, Chi K-W, Chem. Commun 47 (2011) 5184–5186.

[72]. Linares F, Galindo MA, Galli S, Romero MA, Navarro JAR, Barea E, Inorg. Chem 48 (2009) 7413–7420. [PubMed: 19586019]

[73]. Mattsson J, Govindaswamy P, Renfrew AK, Dyson PJ, Štěpnička P, Süss-Fink G, Therrien B, Organometallics 28 (2009) 4350–4357.

[74]. Vajpayee V, Song YH, Yang YJ, Kang SC, Cook TR, Kim DW, Lah MS, Kim IS, Wang M, Stang PJ, Chi K-W, Organometallics 30 (2011) 6482–6489. [PubMed: 22180698]

[75]. Vajpayee V, Song YH, Jung YJ, Kang SC, Kim H, Kim IS, Wang M, Cook TR, Stang PJ, Chi K-W, Dalton Trans. 41 (2012) 3046–3052. [PubMed: 22278716]

[76]. Vajpayee V, Song YH, Yang YJ, Kang SC, Kim H, Kim IS, Wang M, Stang PJ, Chi K-W, Organometallics 30 (2011) 3242–3245. [PubMed: 21779140]

[77]. Vajpayee V, Lee S, Kim S-H, Kang SC, Cook TR, Kim H, Kim DW, Verma S, Lah MS, Kim IS, Wang M, Stang PJ, Chi K-W, Dalton Trans. 42 (2013) 466–475. [PubMed: 23073144]

[78]. Mishra A, Jung H, Park JW, Kim HK, Kim H, Stang PJ, Chi K-W, Organometallics 31 (2012) 3519–3526. [PubMed: 22639481]

[79]. Vajpayee V, Lee SM, Park JW, Dubey A, Kim H, Cook TR, Stang PJ, Chi K-W, Organometallics 32 (2013) 1563–1566 [PubMed: 23580795]

[80]. Lippert B, Wiley-VCH: Weinheim, Germany, (1999).

[81]. Wagstaff AJ, Ward A, Benfield P, Heel RC, Drugs 37 (1989) 162–190. [PubMed: 2649354]

[82]. Raymond E, Chaney SG, Taamma A, Cvitkovic E, Ann. Oncol 9 (1998) 1053–1071. [PubMed: 9834817]

[83]. Grishagin IV, Pollock JB, Kushal S, Cook TR, Stang PJ, Olenyuk BZ, Proc. Natl Acad. Sci. USA 111 (2014) 18448–18453. [PubMed: 25516985]

[84]. Zhang M, Li S, Yan X, Zhou Z, Saha ML, Wang Y-C, Stang PJ, Proc. Natl. Acad. Sci. USA 113 (2016) 11100–11105. [PubMed: 27647900]

[85]. Yu G, Zhang M, Saha ML, Mao Z, Chen J, Yao Y, Zhou Z, Liu Y, Gao C, Huang F, Chen X, Stang PJ, J. Am. Chem. Soc 139 (2017) 15940–15949. [PubMed: 29019660]

[86]. Cao L, Hettiarachchi G, Briken V, Isaacs L, Angew. Chem. Int. Ed 52 (2013) 12033–12037.

[87]. Yu G, Cook TR, Li Y, Yan X, Wu D, Shao L, Shen J, Tang G, Huang F, Chen X, Stang PJ, Proc. Natl. Acad. Sci. USA 113 (2016) 13720–13725. [PubMed: 27856738]

[88]. Yu G, Yu S, Saha ML, Zhou J, Cook TR, Yung BC, Chen J, Mao Z, Zhang F, Zhou Z, Liu Y, Shao L, Wang S, Gao C, Huang F, Stang PJ, Chen X, Nat. Commun 9 (2018) 4335. [PubMed: 30337535]

[89]. Bonnett R, Berenbaum M, Ciba Found. Symp 146 (1989) 40–59. [PubMed: 2697536]

[90]. Lovell JF, Liu TWB, Chen J, Zheng G, Chem. Rev 110 (2010) 2839–2857. [PubMed: 20104890]

[91]. Ethirajan M, Chen Y, Joshi P, Pandey RK, Chem. Soc. Rev 40 (2011) 340–362. [PubMed: 20694259]

[92]. Samanta SK, Moncelet D, Vinciguerra B, Briken V, Isaacs L, Helv. Chim. Acta 101 (2018) e1800057 [PubMed: 31231137]

[93]. Ahmedova A, Momekova D, Yamashina M, Shestakova P, Momekov G, Akita M, Yoshizawa M, Chem. – Asian J 11 (2016) 474–477. [PubMed: 26629785]

[94]. Ahmedova A, Mihaylova R, Momekova D, Shestakova P, Stoykova S, Zaharieva J, Yamashina M, Momekov G, Akita M, Yoshizawa M, Dalton Trans. 45 (2016) 13214–13221. [PubMed: 27488015]

[95]. Mattsson J, Zava O, Renfrew AK, Sei Y, Yamaguchi K, Dyson PJ, Therrien B, Dalton Trans. 39 (2010) 8248–8255. [PubMed: 20689885]

[96]. Yi JW, Barry NPE, Furrer MA, Zava O, Dyson PJ, Therrien B, Kim BH, Bioconjugate Chem. 23 (2012) 461–471.

[97]. Zava O, Mattsson J, Therrien B, Dyson PJ, Chem. – Eur. J 16 (2010) 1428–1431. [PubMed: 20033971]

[98]. Lewis JEM, Gavey EL, Cameron SA, Crowley JD, Chem. Sci 3 (2012) 778–784.

[99]. Schmidt A, Molano V, Hollering M, Pöthig A, Casini A, Kühn FE, Chem. Eur. J 22 (2016) 2253–2256. [PubMed: 26756963]

[100]. Li H, Luo J, Liu T, Chem.–Eur. J 22 (2016) 17949–17952 [PubMed: 27797422]

[101]. Schmidt A, Hollering M, Han J, Casini A, Kühn FE, Dalton Trans. 45 (2016) 12297–12300. [PubMed: 27436541]

[102]. Schmidt A, Hollering M, Drees M, Casini A, Kühn FE, Dalton Trans. 45 (2016) 8556–8565. [PubMed: 27126799]

[103]. Zheng Y-R, Suntharalingam K, Johnstone TC, Lippard SJ, Chem. Sci 6 (2015) 1189–1193 [PubMed: 25621144]

[104]. Fujita M, Oguro D, Miyazawa M, Oka H, Yamaguchi K, Ogura K, Nature 378 (1995) 469–471.

[105]. Harris K, Fujita D, Fujita M, Chem. Commun 49 (2013) 6703–6712.

[106]. Eddaoudi M, Kim J, Wachter JB, Chae HK, O'Keeffe M, Yaghi OM, J. Am. Chem. Soc 123 (2001) 4368–4369 [PubMed: 11457217]

[107]. Zhao D, Tan S, Yuan D, Lu W, Rezenom YH, Jiang H, Wang L-Q, Zhou H-C, Adv. Mater 23 (2011) 90–93. [PubMed: 20972982]

[108]. Tominaga M, Suzuki K, Kawano M, Kusukawa T, Ozeki T, Sakamoto S, Yamaguchi K, Fujita M, Angew. Chem. Int. Ed 43 (2004) 5621–5625.

[109]. Samanta SK, Moncelet D, Briken V, Isaacs L, J. Am. Chem. Soc 138 (2016) 14488–14496. [PubMed: 27723965]

[110]. Datta S, Misra SK, Saha ML, Lahiri N, Louie J, Pan D, Stang PJ, Proc. Natl. Acad. Sci. USA, 115 (2018) 8087–8092. [PubMed: 30038010]

[111]. Allen TM, Cullis PR, Science 303 (2004) 1818–1822. [PubMed: 15031496]

[112]. Samanta SK, Quigley J, Vinciguerra B, Briken V, Isaacs L, J. Am. Chem. Soc 139 (2017) 9066–9074. [PubMed: 28621947]

[113]. Ikemi M, Kikuchi T, Matsumura S, Shiba K, Sato S, Fujita M, Chem. Sci 1 (2010) 68–71.

[114]. Han J, Schmidt A, Zhang T, Permentier H, Groothuis GMM, Bischoff R, Kühn FE, Horvatovich P, Casini A, Chem. Commun 53 (2017) 1405–1408.

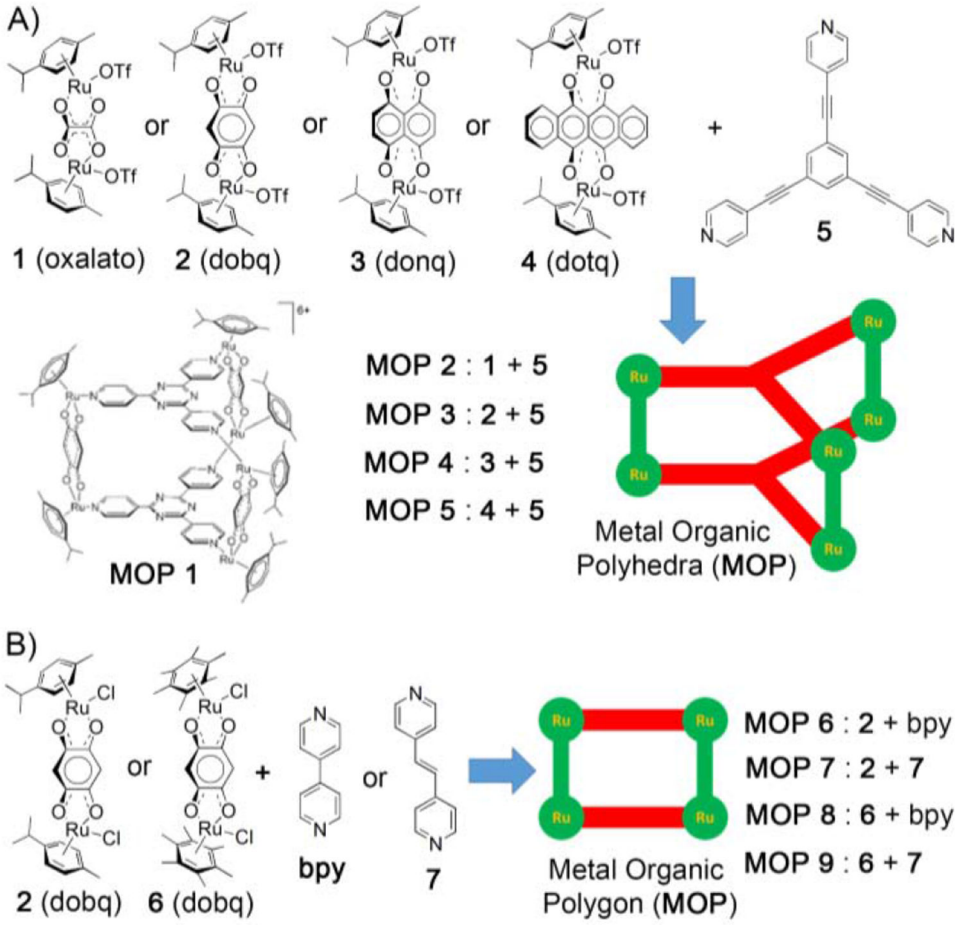

Figure 1:

(A) Metal Organic Polyhedra (**MOP 2-5**) were obtained from [3+2] self-assembly of diruthenium molecular spacers (**1** – **4**) and tritopic ligand (**5**). (B) Metal Organic Polygons (**MOP 6-9**) were obtained from [2+2] self-assembly of diruthenium molecular spacer (**2** or **6**) and ditopic ligand (**bpy** or **7**). (Reprinted by permission from ref. 55. Copyright **2008** from Wiley-VCH).

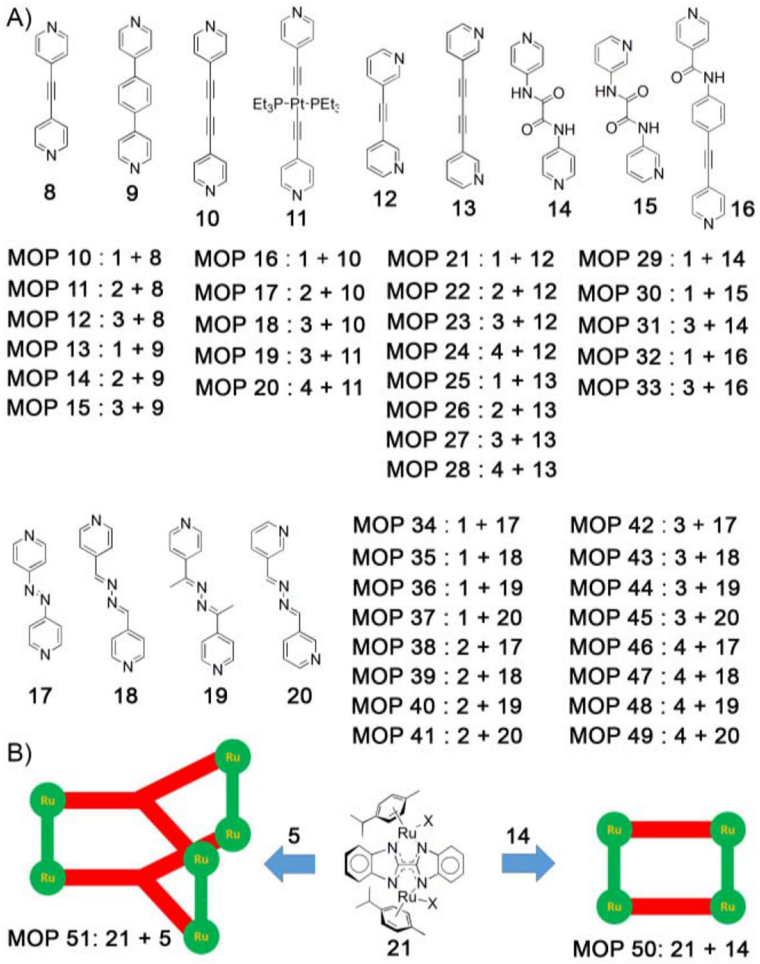

Figure 2:

A) Diruthenium molecular spacers (**1**–**4**) undergo [2+2] self-assembly with ditopic linear donors (**8**–**20**) to give metal organic polygons (**MOPs**). B) Diruthenium molecular spacer (**21**) was used to prepare new class of **MOPs** (**50** and **51**).

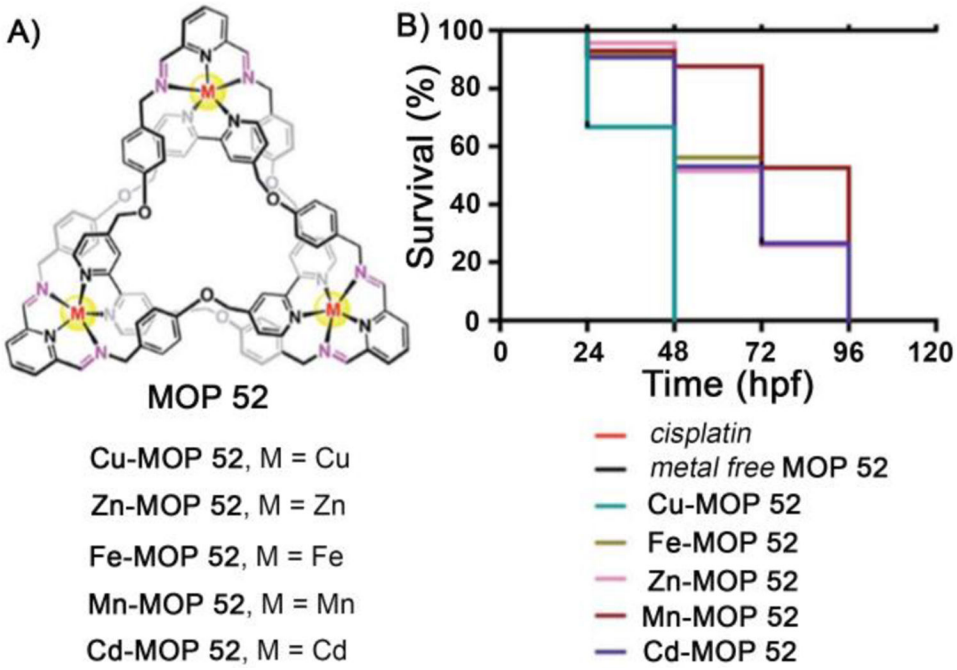

Figure 3:

(a) Chemical structure of **MOP 52**. (b) Kaplan– Meier plot displaying the survival trend after treatment with metallo trefoil knots, *cisplatin*, and metal-free trefoil knots at a fixed concentration of 4 μM. (Reprinted by permission from ref. 34. Copyright **2019** from Royal Society of Chemistry).

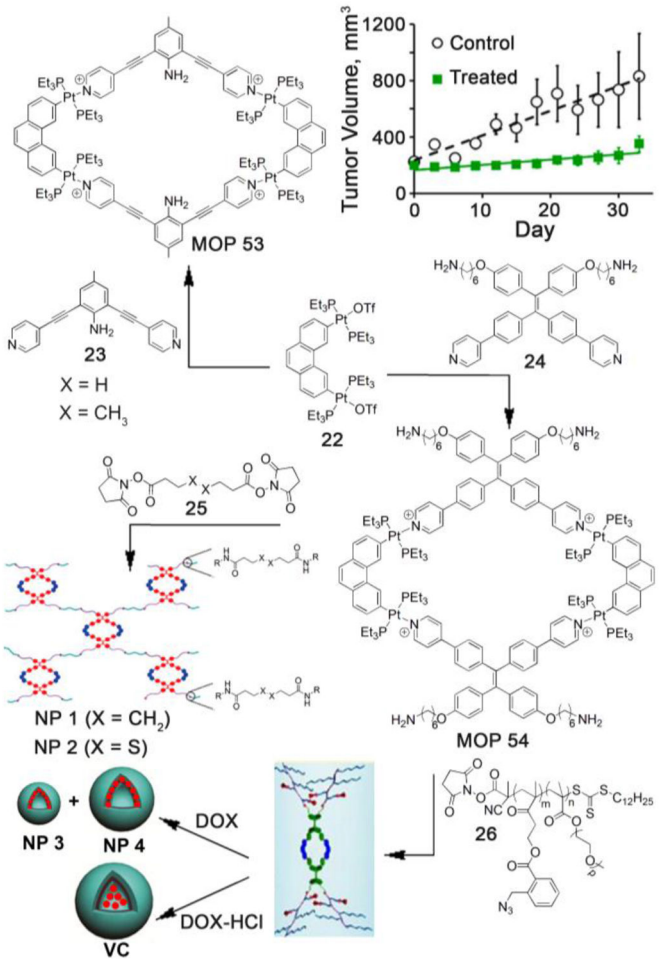

Figure 4:

A) Self-assembly of Pt(II)–based supramolecular polygons (**MOP 53** and **MOP 54**) and their subsequent transformation to prepare supramolecular nanoparticles and vesicles. B) Antitumor study of xenograft tumor bearing mice of breast cancer MDA–MB–231 with **MOP 53**. (Reprinted by permission from ref. 83, 84 and 85. Copyright **2014** and **2016** from National Academy of Sciences and **2017** from American Chemical Society).

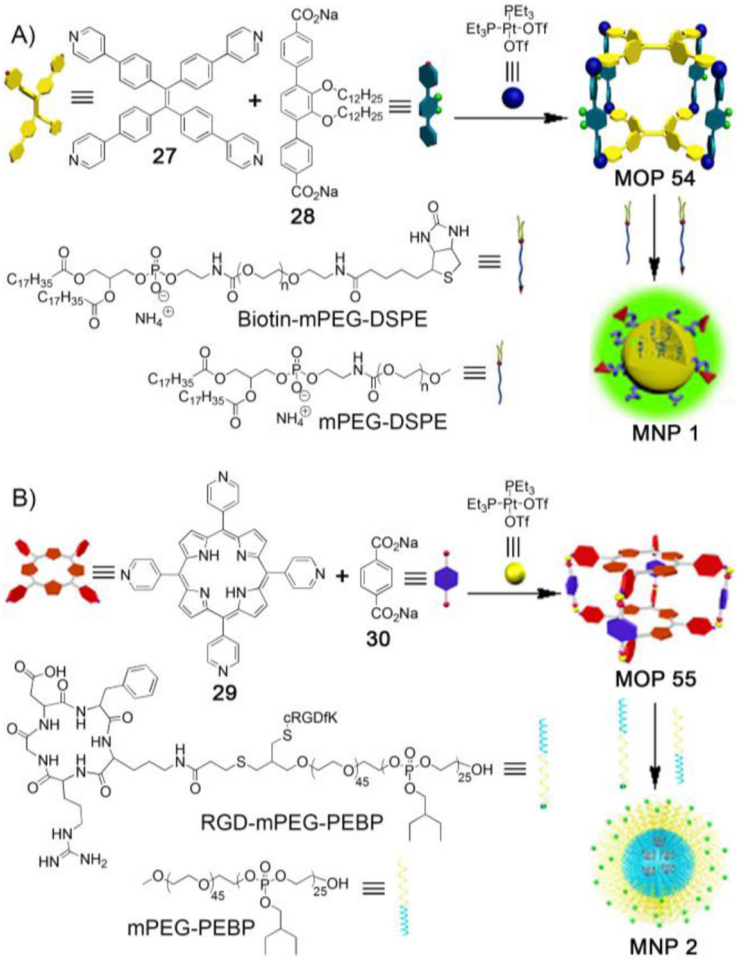

Figure 5:

A) Self–assembly of platinum–based **MOP 55** and its encapsulation within hydrophobic micelles containing cell targeting ligand (biotin) endowing selective delivery of therapeutic platinum–based **MOP 55** to tumor. B) Self–assembly of porphyrin containing platinum–based therapeutic **MOP 56** for combination of chemotherapy and photodynamic therapy. Therapeutic **MOP 56** was delivered after encapsulation within hydrophobic sphere of nanoparticles containing cell targeting ligand (c-RGD). (Reprinted by permission from ref. 87 and 88. Copyright **2016** and **2018** from National Academy of Sciences and Nature Publishing Group).

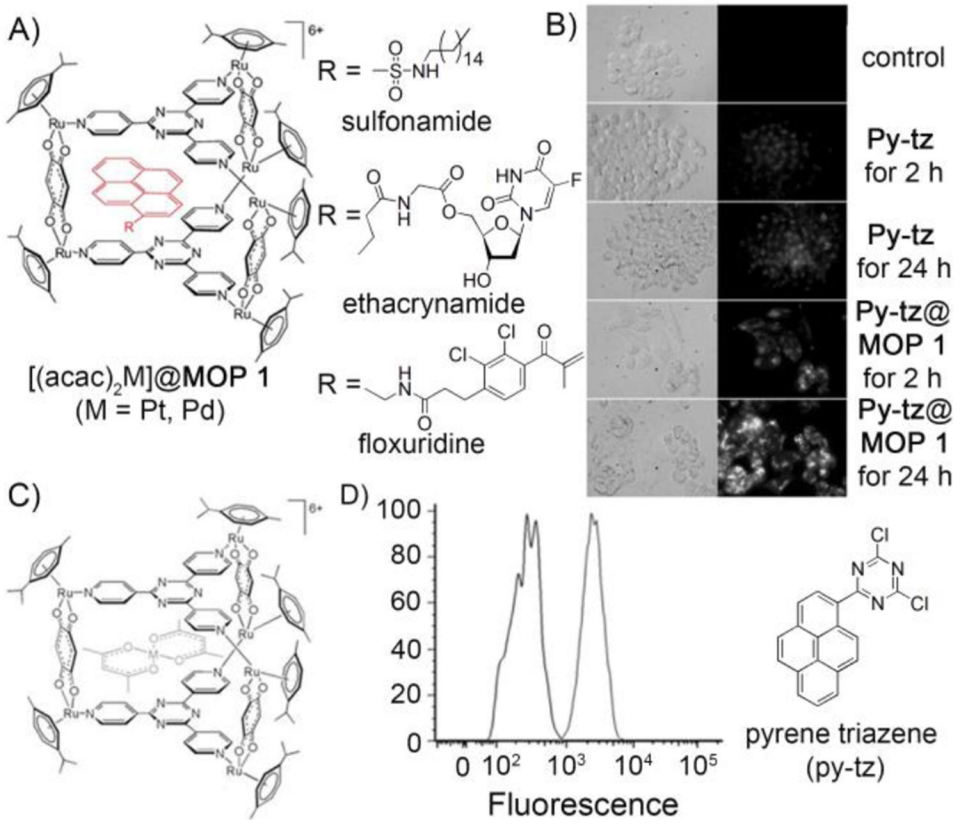

Figure 6.

A) Encapsulation of pyrene derivatives (Pyrene-R) by **MOP 1** to give Pyrene–R@**MOP 1**. B) Microscopy images of cells incubated with py–tz and py–tz@**MOP 1**, transmitted light (left) and fluorescent light (right). C) Molecular structure of [$(acac)_2$Pt@**MOP 1**] obtained from the CCDC (673229) and modified using *Mercury* software. D) Flow cytometry study of A2780 cells treated with Py-tz@**MOP 1** demonstrated transportation and release of Py-tz inside cancer cell. (Reprinted by permission from ref. 55, 95, 96 and 97. Copyright **2008** and **2010** from Wiley-VCH, **2012** from American Chemical Society and **2012** from Royal Society of Chemistry).

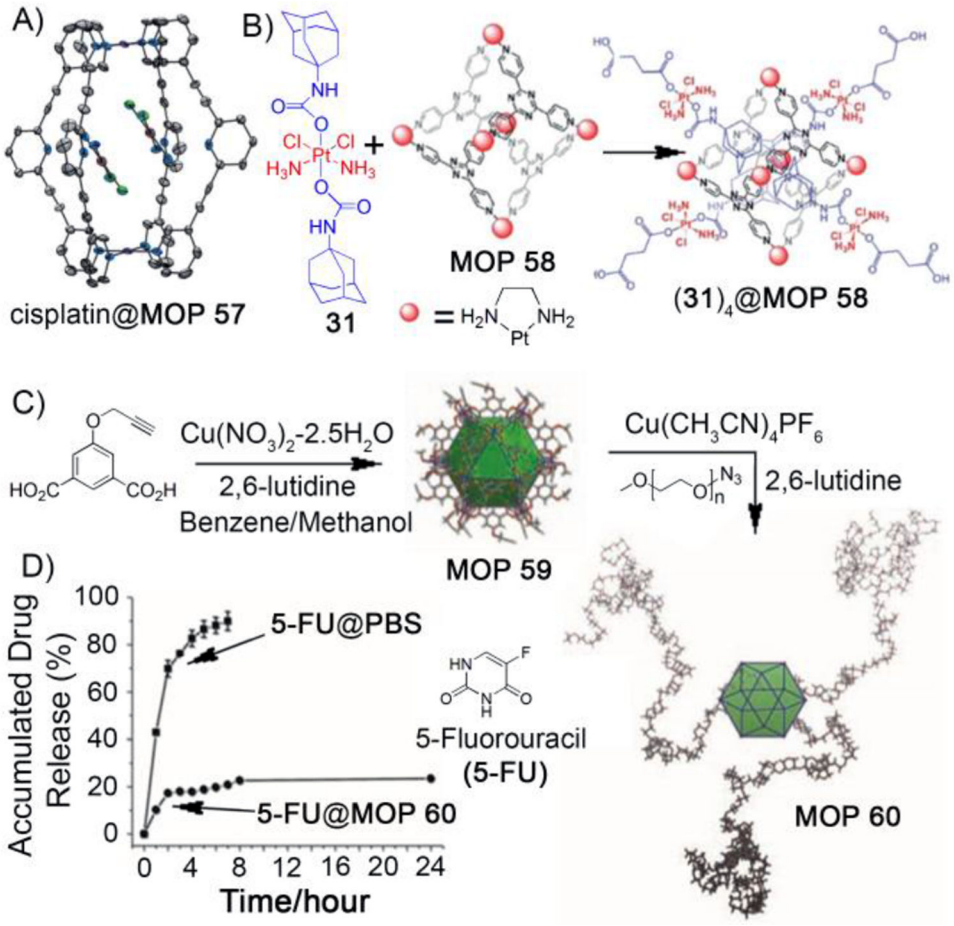

Figure 7:

A) Molecular structure of host–guest complex (cisplatin)$_2$@**MOP 57**. B) Encapsulation of four molecules of platinum prodrugs (31) by **MOP 58** to give (31)$_4$@**MOP 58**. C) Synthesis of copper (II) containing cuboctahedron cage (**MOP 59**) and its surface modification with PEG to give water soluble MOP 60. D) Release profile of 5-fluorouracil (5-FU) from **MOP 60**. (Reprinted by permission from ref. 98, 103 and 107. Copyright **2012** and **2015** from Royal Society of Chemistry, **2011** from Wiley-VCH).

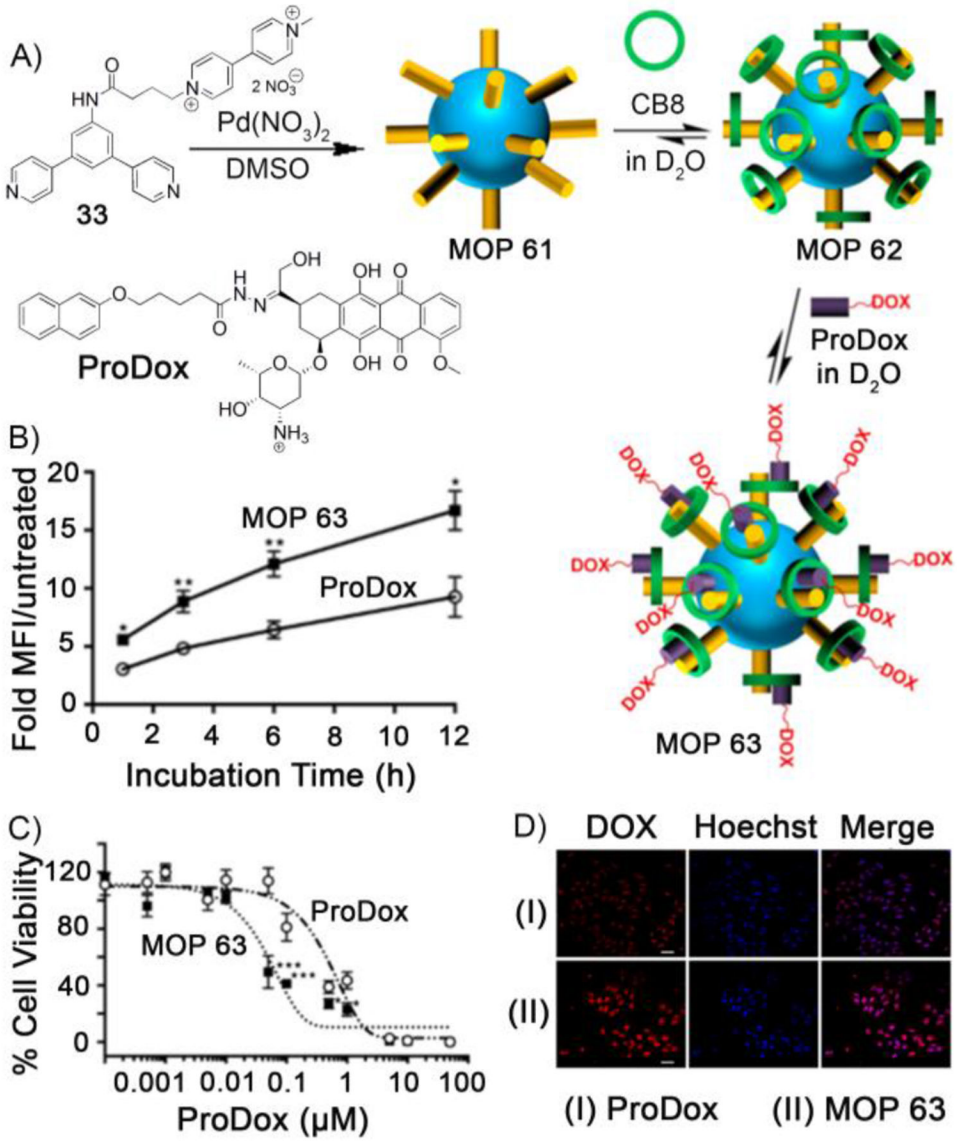

Figure 8.

Self-assembly of methyl viologen–studded **MOP 61** from ligand 33. Capping of **MOP 61** by CB8 followed by drug (ProDox) loading to give **MOP 63**. B) Flow cytometry experiments for HeLa cells treated with **MOP 63** and **ProDox**. C) MTS assay for HeLa cells after treatment with **MOP 63** and **ProDox**. D) Confocal fluorescence microscopy of HeLa cells treated with **MOP 63** and **ProDox**. (Reprinted by permission from ref. 109. Copyright **2016** from American Chemical Society).

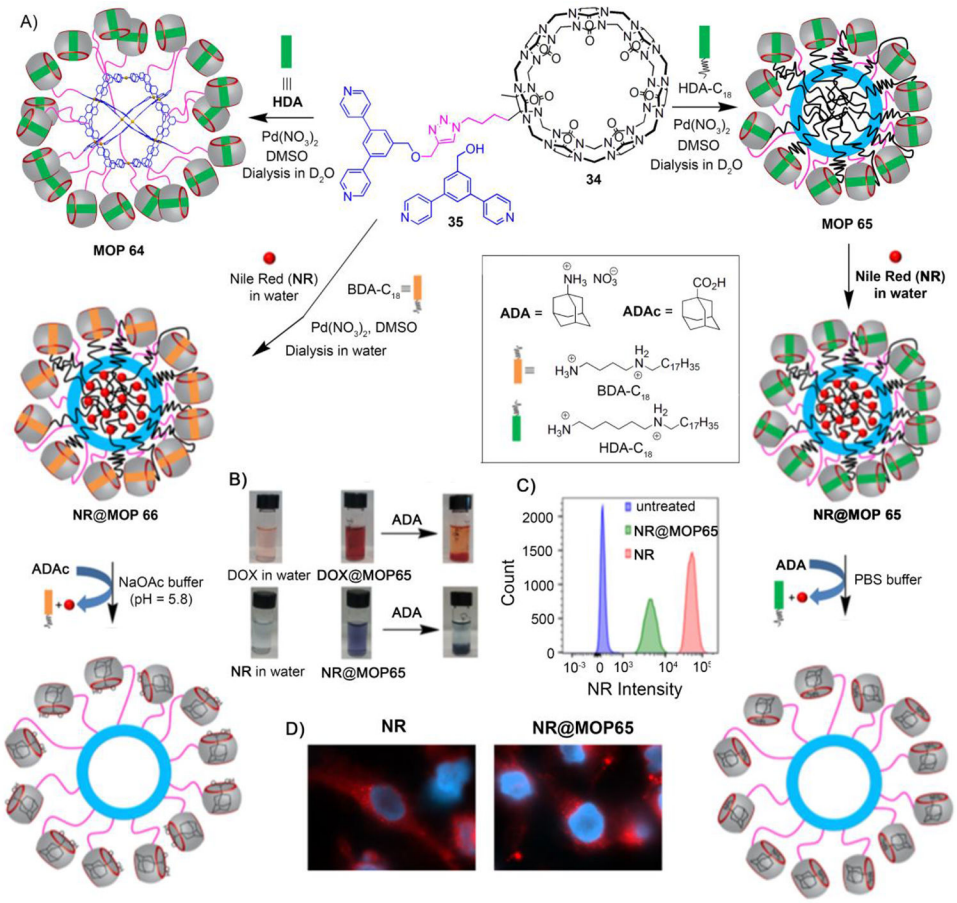

Figure 9:

A) Co-assembly of cucurbit[7]uril–functionalized **MOP 64**. Co-assembly of **MOP 65** and **MOP 66** allow to load with hydrophobic dye nile red (**NR**) inside the cage and stimuli (chemical and pH–chemical) responsive release of **NR**. B) Naked–eye detection of hydrophobic guest (**NR** and **DOX**) encapsulation and chemical–responsive release. C) Flow-cytometry analysis of the uptake of **NR**@**MOP 65** by THP-1 cells. D) Fluorescence microscopy analysis of HeLa cells stained with **NR**@**MOP 65**. (Reprinted by permission from ref. 112. Copyright **2017** from American Chemical Society).

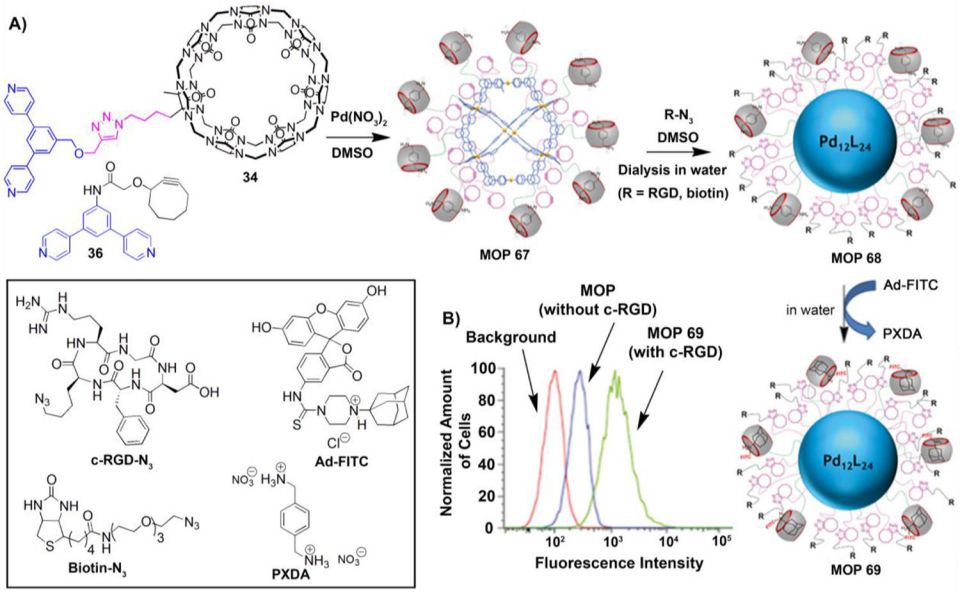

Figure 10:

A) Co–assembly of **MOP 67**. Dual post–synthetic modification of **MOP 67** to give **MOP 69**. B) Flow cytometry uptake study of **MOP 69** (with c–RGD) by U87 cell lines. Inset: chemical structures of c-RGD-N_3, Biotin-N_3, Ad-FITC and PXDA. (Reprinted by permission from ref. 92. Copyright **2018** from Wiley-VCH).

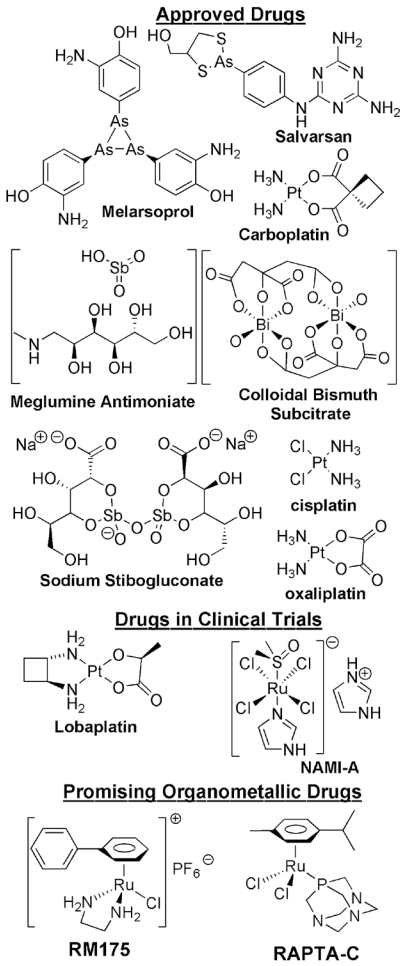

Chart 1.
Approved and promising therapeutic metallodrugs.

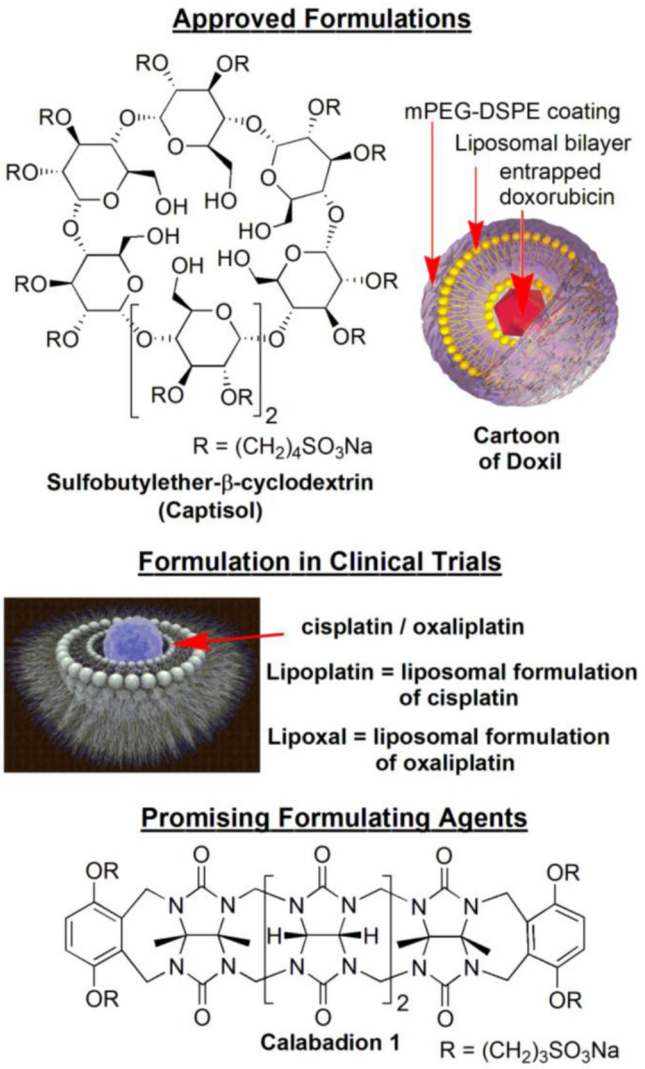

Chart 2:
Approved and promising novel formulating agents.

Table 1.

Cytotoxicities (IC_{50}/μM) of ruthenium–based **MOPs**.

	SK-hep-1	HeLa	HCT-15	A-549	AGS	MDA-MB-231
1 (oxalato)	>200	–	–	–	–	–
2 (dobq)	>200	–	–	–	–	–
3 (donq)	149	–	–	–	–	–
4 (dotq)	>200	–	–	–	–	–
Cisplatin	6.3	10.5	5.6	2.4	>100	2.7
doxorubicin	2.67	3.16	15.34		0.70	
MOP 2	83.7	163.7	187.9	inactive	–	inactive
MOP 4	3.8	9.2	4.1	3.4	–	7.6
MOP 17	114.05	–	109.60	–	31.96	
MOP 18	51.08	14.91	11.40	–	9.61	
MOP 19	58.88	43.71	11.91	–	10.37	
MOP 20	15.45	20.48	15.23	–	11.65	–
MOP 21	5.36	9.40	9.83	–	2.65	–
MOP 22	8.60	9.55	13.27	–	10.83	–
MOP 23	6.97	–	7.46	–	–	–
MOP 24	29.53	–	39.45	–	–	–
MOP 25	66.19	–	53.66	–	–	–
MOP 26	63.58	–	57.05	–	–	–
MOP 27	9.60	–	10.66	–	–	–
MOP 28	16.32	–	17.68	–	–	–
MOP 31	4.2	10.2	3.7	3.2	–	2.8

Table 2.

Cytotoxicities (IC_{50}/μM) of ruthenium–based **MOPs**.

	A-549	Colo320	H1299	MCF7
21	>100	>100	>100	>100
cisplatin	>100	38.6	>100	>100
MOP32	38.86	>100	>100	80.91
MOP33	10.18	0.33	3.62	<0.1
MOP50	13.94	>100	>100	80.91
MOP51	78.86	15.42	15.65	8.41

Table 3.

In vitro and *in vivo* cytotoxicities (IC_{50}/μM) of trefoil knots.

MOPs	Cell lines							Zebrafish Embryo
	HeLa	A2780	A2780 /cis	MDAMB	PC3	MCF-7	HEK-293	
Cu–MOP 52	13.3	3.2	1.3	2.4	27.7	4.8	20.4	4
Zn–MOP 52	5.4	8.3	5.7	6.0	44.5	17.7	11.8	8.8
Fe–MOP 52	1.3	5.2	2.3	3.1	0.9	9.1	>100	8
Cd–MOP 52	1.5	2.1	0.6	1.9	11.7	7.8	16.8	8
Mn–MOP 52	3.3	4.1	4.2	0.8	7.5	3.4	24.3	4.8
Metal-free **MOP 52**	>100	>100	54.6	>100	>100	27.4	>100	>100
cisplatin	25.7	11.2	28.1	16.5	15.4	5.8	1.7	250

Table 4.

Cytotoxicities (IC_{50}) of several host–guest complexes of **MOP 1** towards A2780 cells.

	IC_{50}
$[(acac)_2Pd]$@**MOP 1**	1 μM
$[(acac)_2Pt]$@**MOP 1**	23 μM
[Pyrene-sulfonamide]@**MOP 1**	2 μM
[Pyrene-ethacrynamide]@**MOP 1**	3 μM
[Pyrene-floxuridine]@**MOP 1**	0.3 μM
cisplatin	1.6 μM
MOP 1	23 μM
Py-tz@**MOP 1**	6 μM

Table 5.

Cytotoxicities of cisplatin, **31**, **MOP 58** and (**31**)$_4$@**MOP 58** toward several cell lines.

Cell lines	IC_{50} (μM)			
	cisplatin	**31**	**MOP 58**	**(31)$_4$@MOP 58**
A 549	10.5	50.7	>250	31.5
A2780	1.67	3.58	31.1	4.40
A2780CP70	9.76	22.3	57.7	14.7